Volume **X**, Number **0X**, XX **200X** pp. **X–XX**

A NOVEL MOVING ORTHONORMAL COORDINATE-BASED APPROACH FOR REGION OF ATTRACTION ANALYSIS OF LIMIT CYCLES

Eva Ahbe, Andrea Iannelli, Roy S. Smith

Automatic Control Laboratory, ETH Zürich
Physikstrasse 3, 8092 Zürich, Switzerland

Abstract. The paper proposes a Lyapunov theory-based method to compute inner estimates of the *region of attraction* (ROA) of stable limit cycles. The approach is based on a transformation of the system to transverse coordinates, defined on a *moving orthonormal coordinate system* (MOC) for which a novel construction is presented. The proposed *center point MOC* (cp-MOC) is associated with a user-defined center point and provides flexibility to the construction of the transverse coordinates. In particular, compared to the standard approach based on hyperplanes orthogonal to the flow, the new construction allows the analyst to obtain larger regions of the state space where the well-definedness property of the transformation is satisfied. This has important benefits when using transverse coordinates to compute inner estimates of the ROA. To demonstrate these improvements, a sum-of-squares optimization-based formulation is proposed for computing inner estimates of the ROA of limit cycles for polynomial dynamics described in transverse coordinates. Different algorithmic options are explored, taking into account computational and accuracy aspects. Results are shown for three different systems exhibiting increasing complexity. The presented algorithms are extensively compared, and the newly cp-MOC is shown to markedly outperform existing approaches.

1. **Introduction.** Nonlinear dynamical systems which exhibit periodic steady-state trajectories, or limit cycles, are often encountered in engineering applications, for example robotics [31, 41], power systems [38], aerospace [19], and airborne wind energy [6]. In order to successfully operate these systems, it is paramount to analyze stability of the periodic orbits, and to provide an estimate of the region of the state space from which the system is guaranteed to converge to them. Therefore, computing inner estimates of the region of attraction of the limit cycles is of fundamental importance for the safety of these systems.

Problem setting and past works.

The stability analysis of periodic orbits has a long history, with Poincaré maps presenting the most well-known and established analysis tool. Their appeal is motivated by the fact that the problem of orbital stability of a periodic orbit [17] is reduced to the stability of a fixed point of the map [48]. Thus, asymptotic stability

2020 *Mathematics Subject Classification.* Primary: 93D05, 70K05; Secondary: 90C23.

Key words and phrases. Region of attraction, Lyapunov theory, Sum-of-Squares optimization, Limit Cycles, Moving Orthonormal System, Transverse Dynamics.

This work is supported by the Swiss National Science Foundation under grant no. 200021_178890.

* Corresponding author: iannelli@control.ee.ethz.ch.

conditions based on well-established Lyapunov arguments can be used to verify orbital stability. In [17], the concept of Poincaré maps was extended by considering a *moving orthonormal coordinate system* (MOC) along the trajectory, which can be thought of as moving Poincaré maps. Based on earlier results presented in [46], the moving orthonomal system was proposed in [17] to decompose n-dimensional dynamics into two parts: a transversal part, confined to an (n-1)-dimensional subspace representing a hyperplane transversal to the flow of the system at any given time; and a scalar part, normal to the hyperplane. The coordinates obtained by this transformation are referred to as transverse coordinates. The most common choice of hyperplanes for the transformation are those perpendicular to the system flow. This approach is here referred to as *classical MOC* (class-MOC), and has found extensive application. To name a few examples, this was used: in [18] for constructing periodic quadratic Lyapunov functions for exponentially stable orbits; in [16] for the analysis of the ROA of periodic orbits based on Borg's criterion; and in [25] for formulating generalized criteria for orbital stability. Moreover, application of class-MOC to control various types of nonlinear systems, including hybrid and underactuated systems, can be found in [31, 14, 12].

Motivation.

One of the recognized limitations of the MOC, and as a consequence class-MOC, is that the transformation must fulfil a well-definedness condition which often restricts the portion of the state space where the analysis can be carried out. This aspect, formally presented in Section 2.3, can obviously have detrimental effects when analyzing the ROA of a limit cycle. Indeed, it might be the case that, even though the attractive region of the periodic orbit is large, only small regions around it can be verified because the well-definedness condition is not otherwise fulfilled. A possible remedy for this was investigated in [30], where a nonlinear optimization program aiming at maximizing the well-defined region of the transformation is proposed. Similarly, in [41] an application-specific choice of MOC was proposed which reduces the computational load of the transformation and resulting transverse equations.

Contributions.

Prompted by these shortcomings, the first contribution of this work, presented in Section 3, is the formulation of the *center point MOC* (cp-MOC), that is a novel strategy to construct the MOC which ameliorates the limitations associated with the constraints of the classical transformation. In particular, the proposed cp-MOC allows the analyst to have control over the regions in which the transformation is well-defined. This will be shown by providing an analytical description of the regions, and by pointing out the flexibility with which the regions can be modified.

The second contribution, discussed in Section 4, is the application of this framework to ROA analysis of polynomial nonlinear systems. Algorithms to test the aforementioned sufficient conditions and obtain Lyapunov functions verifying inner estimates of the ROA of the limit cycle are proposed. The computational approach consists of *sum-of-squares* (SOS) programs and are obtained by formulating the Lyapunov conditions as set containment conditions and applying results from semialgebraic geometry. More precisely, the arguments used here are a relaxation of the Positivstellensatz of Stengle [39] in the form of a hierarchy of sufficient SOS conditions for the existence of a polynomial identity which certifies the emptiness of a semialgebraic set [36]. The appeal of SOS is that the condition that one or more polynomials is a sum of square can be equivalently reformulated via *semidefinite*

programs (SDPs). However, by combining the novel cp-MOC for the system analysis with Lyapunov-based stability conditions, bilinear SOS programs are obtained. Therefore, the problem of maximizing inner estimates of the ROA is non-convex, but a coordinate descent approach is employed in order to approximately solve it via iterative convex SDP. Sum-of-squares methods have been widely employed for nonlinear stability analysis [34, 40, 44, 47, 24, 21, 20] and control [22, 37, 9]. The verification of stability regions along trajectories, also referred to as 'funnels', of feedback controlled robotic systems, was obtained from SOS programming in [42, 43, 31, 32, 29]. In order to apply the SOS methods to non-polynomial systems polynomial approximation techniques are explored in [50, 10, 35]. See [11] for a comprehensive overview of applications of SOS programming in these fields. Despite its popularity, the application of SOS to complex control problems is still limited by scalability issues and by the fact that set containment conditions often results in non-nonlinear programs, as noted above. Moreover, an additional source of computational burden is here due to the fact that time-discretization of the periodic orbit is performed, with a consequent increase in the number of optimization variables and constraints in the SOS program. The contribution of this work is the proposal of several algorithmic options, investigated in Section 4, to ameliorate these shortcomings.

Finally, the analysis method is demonstrated in Section 5 by three numerical examples, which all show the benefit of using the cp-MOC in terms of accuracy of the computed ROA. The first two consist of pedagogical systems studied in the nonlinear dynamics literature, namely the Van der Pol oscillator and a modified version of a Liénard system. The third example comes from airborne wind energy systems, which are an emerging renewable energy technology in which tethered kites are used to extract power from the wind. The adopted model has been previously employed for control design of kites in the power-generating flight phase [49, 2].

2. Preliminaries.

2.1. Notation.

Let $\mathcal{P}^n$ denote the ring of all n-variate polynomials with real coefficients and let $\mathcal{P}^n_{\leq r}$ denote its subset containing polynomials of total degree at most $r \in \mathbb{N}_0$. A polynomial $g(x) : \mathbb{R}^n \to \mathbb{R}, g(x) \in \mathcal{P}^n_{\leq r}$ is SOS if it can be written as $g(x) = \sum_i q_i(x)^2$, $q_i(x) \in \mathcal{P}^n_{\leq r/2}$. Moreover, g is SOS if and only if there is a matrix $Q \succeq 0$ such that $g(x) = \mathrm{v}(x)^T Q \mathrm{v}(x)$, where $\mathrm{v}(x)$ is a vector of monomials. The set of all SOS polynomials in the indeterminant x is indicated by $\Sigma[x]$. The degree of a polynomial g in x is indicated by $\partial(g)$. The function $\mathrm{dist}(a, b)$ indicates the distance between two variables $a, b \in \mathbb{R}^n$. Because this is a finite dimensional linear space, any norm can be used to express the distance. The notation $\mathcal{I}_T := [0, T]$ is used to denote closed intervals, and $\mathcal{I}^\circ_T := [0, T)$ is used for half-open intervals. The symbols $\parallel$ ($\nparallel$) are used to indicate parallelism (not parallelism) between two vectors, and $\mathcal{C}^d(\mathbb{R}, \mathbb{R}^n)$ denotes the space of continuous functions from $\mathbb{R}$ to $\mathbb{R}^n$ with continuous derivatives up to order d. We say that $a \in \mathbb{R}^n$ is a unit vector if its Euclidean norm is 1.

2.2. Local stability and region of attraction of periodic orbits.

We consider continuous-time nonlinear dynamics of the form

$$\dot{x} = f(x), \tag{1}$$

where $x \in \mathbb{R}^n$ is the state variable and $f : \mathbb{R}^n \to \mathbb{R}^n$ is the vector field. The function f is assumed to be Lipschitz continuous in x and to have continuous partial derivatives with respect to x.

It is assumed that system (1) has a steady-state consisting of a periodic trajectory, referred to in the remainder as periodic orbit or *limit cycle* (LC), and defined next.

Definition 2.1 ([17] Periodic orbit)**.** Let $\omega(t) : \mathbb{R}^n \to \mathbb{R}$ be a periodic solution of system (1) with period T. A periodic orbit Γ is defined as the closed curve

$$\Gamma = \{x \in \mathbb{R}^n \,|\, x = \omega(t),\, t \in \mathcal{I}_T\}. \tag{2}$$

The curve Γ is invariant with respect to the solutions of (1), and the periodic solution $\omega(t)$ can be obtained from example by considering the flow of the system $\psi(x_{\text{ini}}, t)$ with initial condition $x_{\text{ini}} \in \Gamma$. The periodic orbit Γ is either known analytically or obtained numerically by simulation of (1).

Unlike equilibrium points, for which asymptotic stability is defined by the convergence of all trajectories to one single point, trajectories of a system which converge to a periodic orbit will not converge to a single point, instead to a set. Thus, the notion of *asymptotic orbital stability* is used [17].

Definition 2.2 (Local asymptotic orbital stability)**.** Let $K \subseteq \mathbb{R}^n$ be a region of the state space with $\Gamma \subset K$. An orbit is stable if $\forall \epsilon > 0$, there is a $\delta > 0$ such that $\forall x_{\text{ini}} \in K$ with $\text{dist}(x_{\text{ini}}, \Gamma) < \delta$ it holds $\forall t > 0$ that $\text{dist}(\psi(x_{\text{ini}}, t), \Gamma) < \epsilon$. An orbit is attractive if there is a $\delta > 0$ such that $\forall x_{\text{ini}} \in K$ with $\text{dist}(x_{\text{ini}}, \Gamma) < \delta$ it holds $\lim_{t\to\infty} \text{dist}(\psi(x_{\text{ini}}, t), \Gamma) = 0$. A periodic orbit Γ is called asymptotically orbitally stable if it is stable and attractive.

The *region of attraction* (ROA) of a periodic orbit Γ is defined as

$$\mathcal{R}^* := \{x_{\text{ini}} \in \mathbb{R}^n \,|\, \lim_{t\to\infty} \text{dist}(\psi(x_{\text{ini}}, t), \Gamma) = 0\}, \tag{3}$$

i.e. the set of initial conditions for which the system converges asymptotically to Γ. The goal of this work is to propose computational strategies for the calculation of inner estimates of $\mathcal{R}^*$, that is, guaranteed regions of the state-space for which Γ is attractive.

2.3. **Moving transverse coordinate system.** A pioneering contribution to the study of orbital stability was given in [17], where the concept of MOC was introduced. The basic idea is to decompose the dynamics of the system in the neighborhood of Γ into two parts: the first contains the dynamics on a hyperplane transversal to the trajectory of the limit cycle, and the second represents the dynamics in the direction of the normal to the hyperplane. The construction of the hyperplanes and the associated transformation operator depend on Γ, as discussed later. The two parts of the decomposed dynamics, namely transverse and normal, are then described by two separate sets of coordinates, respectively $\rho \in \mathbb{R}^{n-1}$ and $\tau \in \mathcal{I}_T$, which will be referred to as *transverse coordinates*.

More formally, let $\tau \in \mathcal{I}_T$ be a variable used to parametrize the orbit Γ as

$$\Gamma = \{x \in \mathbb{R}^n \,|\, x = \omega(\tau),\ \tau \in \mathcal{I}_T\}. \tag{4}$$

This implicitly defines a function $\tau(t)$, $-\infty < t < \infty$ which coincides with t on the orbit, i.e. $\frac{d\tau}{dt}\big|_\Gamma = 1$.

The following result from [17] is preparatory for establishing existence of a MOC. We denote by $v : \mathcal{I}_T \to \mathbb{R}^n$ a function associating a unit vector to any point in $\mathcal{I}_T$.

Lemma 2.3 (Lemma 1.1, Section VI.1,[17]). *Given a unit vector function $v : \mathcal{I}_T \to \mathbb{R}^n$ with period T which is Lipschitz continuous. If $n \geq 3$, then there exists a unit vector ζ^* (independent of τ) such that*

$$v(\tau) \neq \pm\zeta^*, \quad \forall\tau. \tag{5}$$

The proof uses the fact that the curve described by any such $v(\tau)$ is rectifiable on a sphere in $\mathbb{R}^n$ and thus covers a set of measure zero. Therefore there always exists a vector ζ^* which is not on this curve or its reverse.

Remark 1. The reason for excluding the case $n = 2$ in Lemma 2.3 lies in the fact that a vector ζ^* is not needed for the construction of a MOC for a 2-dimensional system. This can be seen in the constructive proof of Theorem 2.4, stated next and provided in the Appendix.

In [17], it is suggested to take $v(\tau)$ as the normalized tangent vector to Γ, that is

$$v(\tau) = \frac{f(\omega(\tau))}{\|f(\omega(\tau))\|_2}. \tag{6}$$

The MOC based on this selection of $v(\tau)$ will be referred to in the remainder as *classical MOC* (class-MOC). The proof of its existence is provided in the following theorem.

Theorem 2.4 (Theorem 1.1, Section VI.1, [17]). *Given $\omega \in \mathcal{C}^p(\mathbb{R}, \mathbb{R}^n)$, $p \geq 2$, $\omega(\tau + T) = \omega(\tau)$, $T > 0$, $\frac{d\omega(\tau)}{d\tau} \neq 0$, $0 \leq \tau < T$, and Γ defined in (4). Then, there is a moving orthonormal system along Γ which is $\mathcal{C}^{p-1}(\mathbb{R}, \mathbb{R}^n)$.*

The proof of this theorem is constructive, and is included in the Appendix. Let the vectors defining the class-MOC system be denoted by

$$\mathcal{O}^n = \{v(\tau), \zeta_2(\tau), ..., \zeta_n(\tau)\}. \tag{7}$$

The class-MOC is used to construct a hyperplane "tube" $\mathcal{S} : \mathcal{I}_T \to \mathbb{R}^{n-1}$ around Γ defined as

$$\mathcal{S}(\tau) = \{x \in \mathbb{R}^n | v(\tau)^T (x - \omega(\tau)) = 0\}. \tag{8}$$

such that it satisfies the transversality condition

$$f(\omega(\tau)) \notin \mathcal{S}(\tau), \ \ \forall\tau \in \mathcal{I}_T. \tag{9}$$

This is done by taking the n-1 basis vectors in $\mathcal{O}^n$ orthogonal to $v(\tau)$ to define a transverse projection operator

$$Z(\tau) := [\zeta_2(\tau), ..., \zeta_n(\tau)] \in \mathbb{R}^{n\times(n-1)}. \tag{10}$$

Since $v(\tau)$ is given by (6), $Z(\tau)$ represents the operator projecting onto a moving transverse hyperplane which is orthogonal to the flow of the system at each $\omega(\tau)$. Thus, for any given x in a *sufficiently close* neighborhood of $\omega(t)$, τ specifies the corresponding transversal hyperplane and ρ is the projected position on that hyperplane where $\rho = 0 \Leftrightarrow x = \omega(\tau)$.

The construction of $\mathcal{O}^n$ and the resulting projection $Z(\tau)$ provide the transformation law that maps a state x onto the transverse coordinates (τ, ρ)

$$x = Z(\tau)\rho + \omega(\tau). \tag{11}$$

Critically, this transformation is only locally well-defined. The condition for the transformation to be well-defined can be derived by applying the Implicit Function Theorem.

Lemma 2.5 (Well-definedness condition, Section VI.1, [17])**.** *The transformation* (11) *is well-defined for all* $x \in \mathbb{R}^n$ *in the neighborhood of* Γ *for which the condition*

$$\eta(\tau, \rho) := v(\tau)^T f(\omega(\tau)) + v(\tau)^T \frac{\partial Z(\tau)}{\partial \tau} \rho > 0, \tag{12}$$

is satisfied.

Proof. Consider the algebraic equation $F(x, \tau, \rho) = Z(\tau)\rho + \omega(\tau) - x$. Then the Jacobian with respect to τ, ρ is

$$J = \left[\frac{\partial F}{\partial \tau}, \frac{\partial F}{\partial \rho} \right], \tag{13}$$

where

$$\frac{\partial F}{\partial \tau} = \frac{d\omega(\tau)}{d\tau} + \frac{dZ(\tau)}{d\tau} \rho, \tag{14}$$

$$\frac{\partial F}{\partial \rho} = Z(\tau). \tag{15}$$

Existence of the inverse of J needs to be guaranteed for the transformation to be well-posed, and thus it is required that $\det[J] \neq 0$. Since (15) has rank $n-1$ and $Z(\tau)$ forms an orthonormal system with $v(\tau)$, the following condition results from projecting (14) onto $v(\tau)$

$$v(\tau)^T \left(f(\omega(\tau)) + \frac{\partial Z(\tau)}{\partial \tau}^T \rho \right) \neq 0, \tag{16}$$

for the inverse of J to exist. From the Implicit Function Theorem condition (16) implies well-definedness of the transformation. Specifically, the Lemma prescribes that the left-hand side of (16) be strictly positive. This follows from the following two observations. First, from the definition of $v(\tau)$ (6), one has $v(\tau)^T f(\omega(\tau)) > 0, \forall \tau \in \mathcal{I}_T$. Second, at the origin of $\mathcal{O}^n$ (i.e. for $\rho = 0$), it holds $\frac{\partial Z(\tau)}{\partial \tau}^T \rho = 0$. These two facts thus lead to the condition (12) prescribed by the Lemma. □

It is useful to observe that (12) is affine in ρ for a fixed τ.

Remark 2. When $\eta(\tau, \rho) = 0$, there exists a set of points x for which the transformation (11) is no longer well-defined. An intuition about this set of points can be obtained by the following consideration. Given x, the corresponding coordinate τ of the transformation depends on $\omega(\tau)$ and associated $v(\tau)$ via Eq. (8). If there is more than one $\omega(\tau)$ for which (8) is satisfied then the transformation $x \to (\tau, \rho)$ in (11) is not unique, i.e., it is not well-defined. In the case $n = 2$, this set of points can be visualized as the intersection between neighboring planes orthogonal to the orbit.

3. An improved MOC formulation for ROA analysis of limit cycles.

The standard MOC proposed in [17] has been extensively used in analysis and control of nonlinear systems [18, 16, 25, 30, 14, 12]. However, the well-definedness condition stated in Lemma 2.5 poses a strict upper bound on the region which can be considered in the analyses. Intuitively, and quantitatively shown later in the results, this is a critical limitation when transverse coordinates are used for ROA analysis, as it limits the portion of the state space where property (3) can be verified. In other

words, the inner-estimates cannot go beyond the region for which the transformation is well-defined. In this section, the center point MOC is proposed to addresses the limitations related to the well-definedness conditions of the class-MOC.

3.1. **Formulation of the cp-MOC.** We begin by introducing two notions which are instrumental to define the new coordinate system.

Definition 3.1 (Well-defined "tube")**.** The connected set in which the transformation to a MOC at a given location τ in Γ is well-defined is named the *well-defined region* at τ and is denoted by $\mathcal{V}_\tau$

$$\mathcal{V}_\tau := \{\rho \in \mathbb{R}^{n-1} \,|\, \rho = Z(\tau)^T (x - \omega(\tau)) \,,\, (12) \text{ holds},\ \tau \in \mathcal{I}_T^\circ\}. \tag{17}$$

The union $\mathcal{V} = \bigcup_{\tau \in \mathcal{I}_T^\circ} \mathcal{V}_\tau$ has a tube-like structure and is defined as the *well-defined tube*.

Making use of (11), $\mathcal{V}_\tau$ represents the set of all x located on a given hyperplane $\mathcal{S}(\tau)$ for which (12) holds.

Definition 3.2 (Well-defined MOC)**.** If $\mathcal{V}_\tau \neq \emptyset$ for all $\tau \in \mathcal{I}_T^\circ$ then the MOC is referred to as *well-defined* MOC.

The key observation now is that, as it can be observed in Eqs. (12)-(11), the size of $\mathcal{V}_\tau$ depends on the choice of $v(\tau)$. While in [17] the existence of an MOC (the class-MOC) was shown for the particular choice of $v(\tau)$ in (6), the existence results can be generalized to a broader class of function $v(\tau)$, as is shown in the following.

Corollary 1. *Given a vector function $v : \mathcal{I}_T \to \mathbb{R}^n$ which satisfies Lemma 2.3. If, in addition, it satisfies the condition*

$$v(\tau)^T f(\omega(\tau)) > 0,\ \forall \tau \in \mathcal{I}_T, \tag{18}$$

then there exists a well-defined MOC associated with it.

Proof. Lemma 2.3 guarantees the existence of a vector $\zeta^* \neq \pm v(\tau)$, $\forall \tau$. Using the properties imposed on $v(\cdot)$, Theorem 2.4 proves the existence of an MOC. Thus, the construction of $\mathcal{O}^n$ shown in the proof of Theorem 2.4 (see Eq. (63) in the Appendix) can be directly applied for any such $v(\tau)$. From (18) it follows that the transversality condition (9) holds and thus the operator $Z(\tau)$ given by (10) projects onto a transversal hyperplane representing the desired "tube" around Γ. Further, because (18) holds, the set $\mathcal{V}_\tau$ is non-empty for all τ and thus there exists a neighborhood in which the transformation (11) is well-defined for each $\tau \in \mathcal{I}_T^\circ$ as stated in Lemma 2.5. □

The foregoing discussion points out important features that are desirable for a moving coordinate system and thus should drive the design of a new one. One the one hand, it is advantageous to formulate a lower bound on the size of $\mathcal{V}_\tau$ for all τ and to have the possibility to tune it via design parameters. On the other hand, the variation in the size of $\mathcal{V}_\tau$ over τ would be ideally minimized.

A possible strategy to achieve the first point is to directly maximize the aforementioned lower bound on the size of $\mathcal{V}_\tau$. In [31] the authors propose an optimization problem to obtain a $v(\tau)$ for which the set of ρ where (12) is fulfilled is maximized. The resulting program is, however, non-convex and the result is sensitive to the initial guess. More subtly, there can be choices of $v(\tau)$ for which $\mathcal{V}_\tau$ becomes for some τ practically unbounded (namely when $\frac{\partial Z(\tau)}{\partial \tau}$ goes to zero). This has a twofold

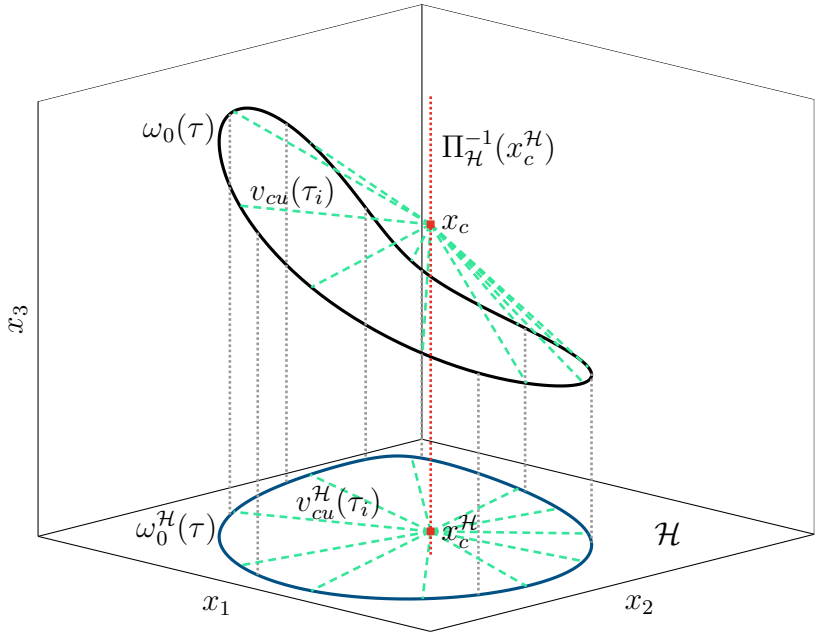

FIGURE 1. Illustration of the orthogonal projection of a notional 3-dimensional periodic orbit with periodic solution ω_0.

consequence: on the one hand, it introduces limitations to the size of $\mathcal{V}_\tau$ for other values of τ; and on the other, it can result in large variations in the size of $\mathcal{V}_\tau$, which in turn can cause numerical problems, particularly in the ROA analysis.

To achieve the aforementioned goals and address the previous limitations, the proposed construction of the novel MOC builds around the choice of a tunable point x_c, which is named here the *center point*. This is a simple (or single) point, and thus, differently from the construction of class-MOC which is defined about a set of points lying on the orbit, the new transverse coordinates depend only on the location of one point. We will therefore refer to it as the *center point MOC* (cp-MOC). The cp-MOC provides explicit knowledge of the $\mathcal{V}_\tau$ for each τ, and makes it possible to directly adjust these regions by means of x_c. In this way, the selection of MOC can be tailored to the particular class of systems, and to the type of analysis performed, which was not previously possible.

We first present the construction of the cp-MOC and the resulting regions $\mathcal{V}_\tau$, and then provide the description of the class of systems for which a cp-MOC can be constructed.

3.2. **Construction of a well-defined cp-MOC.** The algorithm below presents the proposed construction of the vector function $v(\tau)$ used in cp-MOC. Figure 1 depicts a notional limit cycle and schematically illustrates the vectors introduced below.

***Center point algorithm* (CPA):**

Step 1: Compute the normalized tangent vectors $v_t(\tau)$ to $\omega(\tau)$,

$$v_t(\tau) = \frac{f(\omega(\tau))}{\|f(\omega(\tau))\|}. \tag{19}$$

Step 2:

- $n = 2$: Choose a point x_c in the state space inside the area encircled by Γ.
- $n \geq 3$: Choose a point x_c in the state space which lies inside the encircled area obtained from an orthogonal projection of Γ onto a 2-dimensional plane.

Step 3: Construct the normalized vectors $v_c(\tau)$ connecting each point in Γ to the center point x_c

$$v_{cu}(\tau) = -\omega(\tau) + x_c, \tag{20}$$

$$v_c(\tau) = \frac{v_{cu}(\tau)}{\|v_{cu}(\tau)\|}. \tag{21}$$

Step 4:

- $n = 2$: Take $v(\tau) = [-v_{c_2}(\tau), v_{c_1}(\tau)]^T$, where $v_{c_1}(\tau), v_{c_2}(\tau)$ are the components of $v_c(\tau)$.
- $n \geq 3$: Construct a $(n-2)$-dimensional (τ-independent) subspace $\mathcal{N}_f \subseteq \mathbb{R}^{n-2}$ for which the following hold:

$$v_c(\tau) \notin \mathcal{N}_f, \quad v_t(\tau) \notin \mathcal{N}_f, \quad \forall \tau \in \mathcal{I}_T. \tag{22}$$

Compute $v(\tau) \in \mathbb{R}^n$ as the unit vector normal to the subspace generated by span $\{\mathcal{N}_f, v_c(\tau)\}$, for each $\tau \in \mathcal{I}_T$.

$$v(\tau) : \ \left[e_{f_1}, \ \ldots \ e_{f_{n-2}}, \ v_c(\tau)\right]^T v(\tau) = 0, \quad \tau \in \mathcal{I}_T. \tag{23}$$

As long as a subspace $\mathcal{N}_f$ can be found which satisfies the conditions (22) in Step 4, a vector function $v(\tau)$ can be computed from the CPA. However, not all $v(\tau)$ obtained from the CPA result in a well-defined MOC when used as a basis to construct a MOC, as stated in Lemma 2.3 and Theorem 2.4. In particular, both the class of orbits Γ and the choice of x_c in Step 2 can be constraining factors. The conditions for existence of a vector function $v(\tau)$ generated by the CPA algorithm and providing a well-defined MOC are formalized next. First, define

$$\Pi_{\mathcal{H}} : \ \mathbb{R}^n \to \mathbb{R}^2, \tag{24}$$

to be the orthogonal projection onto a 2-dimensional plane $\mathcal{H} \subseteq \mathbb{R}^2$. Then, the set

$$\Gamma^{\mathcal{H}} = \{\omega^{\mathcal{H}} \in \mathbb{R}^2 \,|\, \omega^{\mathcal{H}}(\tau) = \Pi_{\mathcal{H}}\left(\omega(\tau)\right), \ \forall \tau \in \mathcal{I}_T\}, \tag{25}$$

denotes the projected orbit on $\mathcal{H}$.

Theorem 3.3. *Assume that there exists a projection (24) and a point $x_c^{\mathcal{H}} \in \mathcal{H}$ such that there is a bijective map h,*

$$h : \frac{\omega^{\mathcal{H}}(\tau) - x_c^{\mathcal{H}}}{\|\omega^{\mathcal{H}}(\tau) - x_c^{\mathcal{H}}\|} \longrightarrow (1, \varphi), \quad \tau \in \mathcal{I}_T^{\circ}, \ \varphi \in [-\pi, \pi), \tag{26}$$

where φ is the angular coordinate of a point on the unit circle, and

$$\frac{d\varphi}{d\tau} \neq 0 \quad \forall \tau \in \mathcal{I}_T^{\circ}. \tag{27}$$

Then, the vector $v(\tau)$ obtained from the CPA choosing $x_c \in \Pi_{\mathcal{H}}^{-1}(x_c^{\mathcal{H}})$, $x_c < \infty$, results in a well-defined cp-MOC. That is, $\mathcal{V}_\tau \neq \emptyset$, $\forall \tau \in \mathcal{I}_T^{\circ}$.

Proof. Let $v_{cu}^{\mathcal{H}} = -\omega^{\mathcal{H}}(\tau) + x_c^{\mathcal{H}}$ indicate the vectors connecting each element in $\Gamma^{\mathcal{H}}$ to $x_c^{\mathcal{H}}$. From the existence of the bijective map h onto the polar coordinates of a unit circle, i.e., $h\left(\frac{-v_{cu}^{\mathcal{H}}(\tau_i)}{\|v_{cu}^{\mathcal{H}}(\tau_i)\|}\right) = \varphi_i$ with a unique φ_i for each τ_i, it follows that

$$v_{cu}^{\mathcal{H}}(\tau_i) \nparallel v_{cu}^{\mathcal{H}}(\tau_j) \quad \forall \tau_i, \tau_j \in \mathcal{I}_T^\circ,\ i \neq j. \tag{28}$$

Let $f^{\mathcal{H}}$ denote the dynamics projected onto $\mathcal{H}$. From (28) and (27) follows that

$$f^{\mathcal{H}}\left(\omega^{\mathcal{H}}(\tau)\right) \nparallel \pm v_{cu}^{\mathcal{H}}(\tau), \quad \forall \tau \in \mathcal{I}_T^\circ, \tag{29}$$

This can be shown by contradiction. If $f^{\mathcal{H}}(\omega^{\mathcal{H}}(\tau_i)) \parallel \pm {v_{cu}}^{\mathcal{H}}(\tau_i)$ for a $\tau_i \in \mathcal{I}_T^\circ$, then either of the following holds. There is a symmetry in $\omega^{\mathcal{H}}(\tau)$ with respect to $v_{cu}^{\mathcal{H}}(\tau)$, and thus there exist τ_i and τ_j for which $\frac{-v_{cu}^{\mathcal{H}}(\tau_i)}{\|v_{cu}^{\mathcal{H}}(\tau_i)\|} = \frac{-v_{cu}^{\mathcal{H}}(\tau_j)}{\|v_{cu}^{\mathcal{H}}(\tau_j)\|}$, which would contradict (28). There exists a saddle-point in the mapping, that is a point where $\frac{d\varphi}{d\tau} = 0$, which would contradict (27).

From (29) it follows that $f(\omega(\tau)) \nparallel \pm v_c(\tau)$, $\forall \tau \in \mathcal{I}_T^\circ$, where $v_c(\tau)$ is in defined (21) where x_c is any element in the set given by the inverse projection $\Pi_{\mathcal{H}}^{-1}(x_c^{\mathcal{H}})$. The function $v_c(\tau)$ then allows the computation of a constant $(n\text{-}2)$-dimensional subspace $\mathcal{N}_f$ satisfying the conditions stated in Step 4 of the CPA, and the computation of $v(\tau)$ as in (23) for which results $v(\tau)^T f(\omega(\tau)) > 0$, $\forall \tau \in \mathcal{I}_T^\circ$, and thus $\mathcal{V}_\tau \neq \emptyset$, $\forall \tau \in \mathcal{I}_T^\circ$. □

Remark 3. Theorem 3.3 provides sufficient conditions, depending on the particular shape of the orbit, such that a well-defined cp-MOC is guaranteed to exist. This result also shows that theoretically the cp-MOC can be constructed from any finite $x_c \in \Pi_{\mathcal{H}}^{-1}(x_c^{\mathcal{H}})$. In the notional example of Fig. 1, any x_c on the vertical red dotted line would be a valid choice. However, for numerical reasons it is often beneficial to choose a $x_c \in \Pi_{\mathcal{H}}^{-1}(x_c^{\mathcal{H}})$ which lies close to the orbit Γ, e.g., its centroid.

Theorem 3.3 provides a sufficient condition for the cp-MOC to be well-defined in terms of x_c. This is important as it provides formal guarantees for an admissible construction of $v(\tau)$, and thus of the MOC, based on the center point. In practice, the well-definedness of a cp-MOC can be ascertained by checking the conditions of Corollary 1, which are directly in terms of $v(\tau)$. Since $v(\tau)$ is continuous by construction, the remaining condition to check is (18).

Remark 4. As it will be discussed in Section 4, to numerically estimate the region of attraction of the limit cycle we will restrict attention to polynomial vector field. In this case, checking (18) amounts to computing the zeros of the polynomial $v(\tau)^T f(\omega(\tau))$, $\tau \in \mathcal{I}_T^\circ$, after all steps up to Step 4 in the Center point algorithm have been completed. If the polynomial has no zeros then the cp-MOC constructed from the obtained $v(\tau)$ is well-defined. If the polynomial has one or more zeros, then the algorithm can be repeated for a different choice of x_c. Often, existing information on the shape of the orbit can be helpful in finding a suitable x_c from geometrical considerations.

An important feature of the cp-MOC is that it allows an analytical expression for the sets $\mathcal{V}_\tau$ to be obtained, as stated next.

Corollary 2. *For a cp-MOC, the set $\mathcal{V}_\tau$ for each $\tau \in \mathcal{I}_T^\circ$ is given by the open half space containing $\rho = 0$ and resulting from the subtraction of the $(n\text{-}2)$-dimensional hyperplane $\mathcal{S}_{\mathcal{V}_\tau}(\tau)$ generated by span$\left\{ Z(\tau)^T \left(v_{c_u}(\tau) + ker\left(\frac{\partial v(\tau)}{\partial \tau}\right)\right)\right\}$ from the $(n\text{-}1)$-dimensional subspace $\mathcal{S}(\tau)$.*

Proof. As stated in Definition 3.1, for a $\tau \in \mathcal{I}_T^\circ$ the set $\mathcal{V}_\tau$ is given by all $\rho \in \mathbb{R}^{n-1}$ for which the well-definedness condition (12) is satisfied. Eq. (12) is an affine equation in ρ for a given τ, and thus the well-defined region is limited by the ρ at which the condition (12) is no longer satisfied, i.e. by the ρ for which $\eta(\rho,\tau) = 0$. Because the hyperplane $\mathcal{S}_{\mathcal{V}_\tau}(\tau)$ is located by definition at the boundary of the well-defined region, it is associated with the condition $\eta(\rho,\tau) = 0$. This implies, according to (12), that

$$v(\tau)^T f(\omega(\tau)) + v(\tau)^T \frac{\partial Z(\tau)}{\partial \tau}\rho = 0. \tag{30}$$

Rewriting the partial derivative in (30) yields

$$\begin{aligned}
& v(\tau)^T f(\omega(\tau)) + \frac{\partial}{\partial \tau}\left(v(\tau)^T Z(\tau)\right)\rho - \frac{\partial v(\tau)^T}{\partial \tau} Z(\tau)\rho = 0, \\
\implies & v(\tau)^T f(\omega(\tau)) - \frac{\partial v(\tau)^T}{\partial \tau} Z(\tau)\rho = 0, \qquad (\text{since } v(\tau)^T Z(\tau) = 0), \\
\implies & v(\tau)^T f(\omega(\tau)) - \frac{\partial v(\tau)^T}{\partial \tau}\left(x - \omega(\tau)\right) = 0, \qquad \text{from (11)}, \\
\implies & \frac{\partial v(\tau)^T}{\partial \tau} x = v(\tau)^T f(\omega(\tau)) + \frac{\partial v(\tau)^T}{\partial \tau}\omega(\tau), \\
& \qquad = \frac{\partial}{\partial \tau}\left(v(\tau)^T \omega(\tau)\right), \\
& \qquad = \frac{\partial}{\partial \tau}\left(v(\tau)^T \left(-v_{c_u}(\tau) + x_c\right)\right), \qquad \text{from (20)}, \\
& \qquad = \frac{\partial}{\partial \tau}\left(v(\tau)^T x_c\right), \qquad \text{since } v(\tau)^T v_{cu}(\tau) = 0 \text{ by construction}, \\
& \qquad = \frac{\partial v(\tau)^T}{\partial \tau} x_c, \qquad \text{since } x_c = \text{const}.
\end{aligned}$$

The equality

$$\frac{\partial v(\tau)^T}{\partial \tau} x = \frac{\partial v(\tau)^T}{\partial \tau} x_c, \tag{31}$$

is satisfied by all x such that

$$x = x_c + \ker\left(\frac{\partial v(\tau)^T}{\partial \tau}\right). \tag{32}$$

Substituting (32) in (11) and solving for ρ results in

$$\begin{aligned}
\rho|_{\eta(\tau,\rho)=0} &= Z(\tau)^T \left(x_c - \ker\left(\frac{\partial v(\tau)^T}{\partial \tau}\right) - \omega(\tau)\right), \\
&= Z(\tau)^T \left(v_{c_u}(\tau) - \ker\left(\frac{\partial v(\tau)^T}{\partial \tau}\right)\right), \qquad (\text{from (20)}).
\end{aligned} \tag{33}$$

Due to the linearity of $\eta(\tau,\rho)$ in ρ and $\rho = 0 \Rightarrow \eta(\tau,0) > 0$, the condition (12) holds for all ρ in the half space which contains $\rho = 0$ and is given by the subtraction of the hyperplane $\mathcal{S}_{\mathcal{V}_\tau}(\tau) := \rho|_{\eta(\tau,\rho)=0}$ from $\mathcal{S}(\tau)$. □

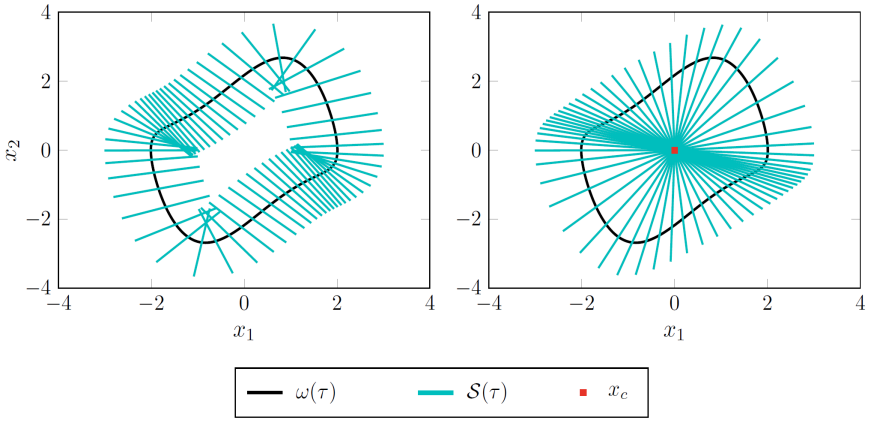

FIGURE 2. *Left plot:* Illustration of the hyperplanes $\mathcal{S}(\tau)$ given by the class-MOC for the limit cycle of the Van der Pol oscillator. *Right plot:* Illustration of the hyperplanes $\mathcal{S}(\tau)$ given by the cp-MOC with $x_c = [0, 0]^T$ for the limit cycle of the Van der Pol oscillator.

Remark 5. For $n = 2$, the sets $\mathcal{V}_\tau$ given by Corollary 2 is the 1-dimensional open half space containing $\rho = 0$, which is given by the intersection of $\mathcal{S}(\tau)$ with the center point x_c.

To provide a pictorial interpretation of the results, Figure 2 illustrates the hyperplanes obtained in a class-MOC and in a cp-MOC for a planar example. As stated in Remark 2, the regions $\mathcal{V}_\tau$ are limited by the point of intersection of two neighboring hyperplanes. The hyperplanes for the class-MOC (left plot) show that, in the inner part of Γ, this results in significantly smaller regions at locations of large curvature of Γ compared to locations of small curvature. In contrast, the hyperplanes for the cp-MOC reveal a unique intersection point at x_c which defines the limit of the regions $\mathcal{V}_\tau$ as described by Corollary 2. This illustration showcases how the cp-MOC is able to provide well-defined regions $\mathcal{V}_\tau$ with more uniform size. Moreover, it is possible to infer from the figure that, by changing the location of x_c, the size of the sets $\mathcal{V}_\tau$ can be changed with a certain degree of flexibility.

3.3. **Transverse coordinate dynamics.** Consider the nonlinear dynamics (1) and let x satisfy the transformation equation (11) obtained from a well-defined MOC (class-MOC or cp-MOC are two particular cases). The dynamics in the transverse coordinate (τ, ρ) are then obtained by considering

$$\frac{dZ(\tau)}{d\tau}\dot{\tau}\rho + Z(\tau)\dot{\rho} + f(\omega(\tau))\dot{\tau} = f(Z(\tau)\rho + \omega(\tau), \vartheta). \tag{34}$$

Projecting both sides of (34) onto $v(\tau)$ gives the 1-dimensional *normal* dynamics:

$$\dot{\tau} = \frac{v(\tau)^T f(\omega(\tau) + Z(\tau)\rho, \vartheta)}{v(\tau)^T f(\omega(\tau)) + v(\tau)^T \frac{\partial Z(\tau)}{\partial \tau}\rho}, \tag{35}$$

where (18) was used. Inspection of (35) reveals the denominator to be equal to the left hand side in (12). Let us thus define $\dot{\tau}(\tau,\rho) = \frac{\mu(\tau,\rho)}{\eta(\tau,\rho)}$, with

$$\mu(\tau,\rho) := v(\tau)^T f(\omega(\tau) + Z(\tau)\rho). \tag{36}$$

Further, projecting both sides of (34) onto $Z(\tau)$ gives the (n-1)-dimensional *transverse* dynamics:

$$\dot{\rho} = \frac{dZ(\tau)}{d\tau}\dot{\tau}Z(\tau)\rho + Z(\tau)^T f(\omega(\tau) + Z(\tau)\rho, \vartheta) - Z(\tau)^T f(\omega(\tau))\dot{\tau}. \tag{37}$$

Note that in the case of class-MOC, $Z(\tau)^T f(\omega(\tau)) = 0$, and thus the second term in the right-hand side of (37) is equal to 0.

4. Region of attraction analysis of limit cycles in transverse coordinates.

This section presents a computational approach to numerically estimate the ROA of limit cycles. The approach is based on Lyapunov theory arguments formulated with respect to dynamical systems transformed into transverse coordinates, for which the new formulation developed in Section 3 is leveraged. Whereas the results were presented therein for a more general class of vector fields (which only need to satisfy the assumptions of continuity and differentiability), we restrict the attention here to polynomial functions f. A numerical procedure based on SOS is then proposed to compute verifiable inner estimates of the ROA.

4.1. Lyapunov criteria for the ROA of a limit cycle.

Conditions to characterize the local stability of periodic orbits in the context of transverse coordinates were first proposed in [30]. In the following, the notation $\mathcal{I}_T^\circ$ is used to denote, given the period T, the half-open time interval $[0, T)$.

Theorem 4.1. [30, Theorem 2]
Let $V : \mathcal{I}_T \times \mathbb{R}^{n-1} \to \mathbb{R}$ be a function that is piecewise continuously differentiable in τ and continuously differentiable in ρ, and such that $\mathcal{R} := \{(\tau,\rho) \in \mathcal{I}_T^\circ \times \mathbb{R}^{n-1} \mid V(\tau,\rho) \leq \gamma\}$ is a compact set, where $\gamma > 0$ is a constant. If V satisfies:

$$V(\tau,\rho) > 0, \quad \forall (\tau,\rho) \in \mathcal{R}, \rho \neq 0, \tag{38}$$

$$\dot{V}(\tau,\rho) = \frac{\partial V(\tau,\rho)}{\partial \rho}\dot{\rho} + \frac{\partial V(\tau,\rho)}{\partial \tau}\dot{\tau} < 0, \quad \forall (\tau,\rho) \in \mathcal{R}, \rho \neq 0, \tag{39}$$

$$V(\tau,0) = \dot{V}(\tau,0) = 0, \quad \forall \tau \in \mathcal{R}, \tag{40}$$

$$\eta(\tau,\rho) > 0, \quad \forall (\tau,\rho) \in \mathcal{R}, \tag{41}$$

where $\eta(\tau,\rho)$ is as defined in (12), then $\mathcal{R} \subseteq \mathcal{R}^*$. That is, $\mathcal{R}$ is an inner estimate for the ROA of Γ.

The proof uses classic Lyapunov arguments. From the Lipschitz assumption on f and (41) it follows that trajectories (τ,ρ) of the system starting from $\mathcal{R}$ exist and are unique. Equations (38)-(39) guarantee that $\mathcal{R}$ is invariant. Finally, Eq. (40) implies that trajectories starting in $\mathcal{R}$ all have the property $\rho \to 0$ as $t \to \infty$. From this, it follows that Γ is locally asymptotically orbitally stable and $\mathcal{R}$ is an inner estimate of the region of attraction.

In the following we restrict V to be polynomial in both τ and ρ. Using the transverse dynamics (37) and (35), condition (41) results in

$$\frac{\partial V(\tau,\rho)}{\partial \rho}\left[\frac{dZ(\tau)}{d\tau}^T \dot{\tau} Z(\tau)\rho + Z(\tau)^T f(\omega(\tau)+Z(\tau)\rho)\dot{\tau} - Z(\tau)^T f(\omega(\tau))\dot{\tau}\right] + \frac{\partial V(\tau,\rho)}{\partial \tau}\dot{\tau} < 0. \tag{42}$$

Equation (35) reveals that the left hand side in the condition (42) contains rational terms. Since the denominator term, $\eta(\tau,\rho)$, is, however, constrained to be positive in order for the transverse coordinate transformation to be well defined, it is possible to multiply both sides of (42) by $\eta(\tau,\rho)$. This results in the polynomial inequality condition

$$\begin{aligned}\frac{\partial V(\tau,\rho)}{\partial \rho}\Bigg[\frac{dZ(\tau)}{d\tau}^T \mu(\tau,\rho) Z(\tau)\rho + Z(\tau)^T f(\omega(\tau) \\ + Z(\tau)\rho)\eta(\tau,\rho) - Z(\tau)^T f(\omega(\tau))\mu(\tau,\rho)\Bigg] + \frac{\partial V(\tau,\rho)}{\partial \tau}\mu(\tau,\rho) < 0.\end{aligned} \tag{43}$$

If we replace (41) by (43), the constraints in Theorem 4.1 are now all polynomial and thus are amenable to be solved using tools from polynomial optimization.

4.2. **Algorithms for an inner estimate of the ROA of the orbit.** The conditions (38), (39), (40) and (43) on the set $\mathcal{R}$ can be reformulated as semialgebraic set containment conditions. In the following, an optimization problem is presented to maximize the size of $\mathcal{R}$. This program is obtained by using classic Positivstellensatz arguments for which computationally tractable relaxations are available [36]. Specifically, they provide the set containment conditions in the form of SOS constraints.

The resulting prototypical optimization problem that needs to be solved is non-convex, and is in the form of a SOS program with bilinear terms in the decision variables.

$$\max_{V,s_1,s_2} \quad \text{volume}\,(\mathcal{R}) \tag{44a}$$

subject to

$$V(\tau,\rho) - l(\rho) \in \Sigma[\tau,\rho], \tag{44b}$$

$$-\dot{V}(\rho,\tau) - (\gamma - V(\tau,\rho))s_1(\tau,\rho) - l(\rho) \in \Sigma[\tau,\rho], \tag{44c}$$

$$\eta(\rho,\tau) - (\gamma - V(\tau,\rho))s_2(\tau,\rho) \in \Sigma[\tau,\rho], \tag{44d}$$

$$s_1(\tau,\rho),\ s_2(\tau,\rho) \in \Sigma[\tau,\rho], \tag{44e}$$

where s_1 and s_2 are so-called SOS multipliers. The addition of $l(\rho) = \epsilon\rho^T\rho$ with $\epsilon \ll 1$ in (44b) is used to enforce strict inequality constraints, and (44d)-(44c) certify that the inequality constraints (38)-(39) hold. This follows from standard SOS arguments, and the reader is referred to [34, 45] for concise reviews of SOS techniques and their application to enforce set containment conditions. Note that in general (44b) enforces a stricter constraint on the function V, which is only required to be positive semidefinite inside of its γ-sublevel set, to improve the numerical robustness of the computations.

Because of the particular application considered here, there are various possibilities for the choice of Lyapunov function V and for the cost function in (44a), in particular regarding the implementation of the time-varying nature of V. These choices are very important, as they have a strong influence on the computational complexity and on the size of the certified set $\mathcal{R}$. Driven by the objective to maximize $\mathcal{R}$, possible choices for Lyapunov functions and cost functions, referred to as *algorithmic options*, are investigated in the following, ordered by increasing complexity.

4.2.1. *Scaling the sublevel set of a pre-computed V (referred to as VSS-∂_{lin}).* A Lyapunov function for an asymptotically orbitally stable periodic orbit Γ can be directly obtained by solving the periodic Lyapunov equation presented in [18] (and, in more general form, in [7]). The periodic Lyapunov equation is a generalization of Lyapunov's Indirect Method to periodic solutions. It requires the linearization of the transverse dynamics (37) and (35) of system (1) around $\omega(\tau)$ (i.e., $\rho = 0$). The transverse linearization associated with (1) is

$$\begin{aligned} A_{\mathcal{S}}(\tau) = \left[\frac{d}{dt} Z(\tau)^T\right] Z(\tau) + Z(\tau)^T \frac{\partial f(\omega(\tau))}{\partial x} Z(\tau) \\ - Z(\tau)^T f(\omega(\tau)) \frac{v(\tau)^T \frac{\partial f(\omega(\tau))}{\partial x} Z(\tau) - v(\tau)^T \frac{\partial Z(\tau)}{\partial t}}{v(\tau)^T f(\omega(\tau))}. \end{aligned} \tag{45}$$

The periodic Lyapunov equation can then be written as

$$\dot{P}(\tau) + A_{\mathcal{S}}(\tau)^T P(\tau) + P(\tau) A_{\mathcal{S}}(\tau) + H(\tau) = 0, \tag{46}$$

where $H(\tau) \succ 0$ is a continuous positive definite T-periodic matrix. Once a user-defined $H(\tau)$ has been chosen [18, Theorem 2.2], one can solve (46) to obtain the unique periodic solution $P(\tau) \succ 0$. The Lyapunov function

$$V(\tau, \rho) = \rho^T P(\tau) \rho, \tag{47}$$

can then be used in (44) where the objective is to maximize the sublevel set size γ. The associated optimization problem is

$$\max_{\gamma, s_1, s_2} \quad \gamma, \tag{48a}$$

$$\text{subject to} \quad (44b), (44c), (44d), (44e). \tag{48b}$$

The drawback of this strategy, originally presented in [31], is that the shape of the inner estimate, which is an important degree of freedom when computing inner estimates of the ROA, is set to the solution of (46) and can not be optimized over. Moreover, the choice is limited to quadratic functions, which again limits the flexibility of the algorithm.

4.2.2. *Scaling the sublevel set and optimizing the shape of a quadratic V (referred to as VSS-$\partial(2)$).* To partially ameliorate these shortcomings, one can parametrize the Lyapunov function as a quadratic form with a τ-varying Gram matrix

$$V(\tau, \rho) = \rho^T Q(\tau) \rho, \tag{49}$$

where $Q(\tau)$ is linear in τ. In order to prevent an artificial increase of the sublevel set size by a rescaling of $Q(\tau)$ (with no effect on the computed region), the trace of

$Q(\tau)$ is set to a constant value $c > 0$ at each $\tau \in \mathcal{I}_T^\circ$. The associated optimization problem is

$$\begin{aligned} \max_{s_1, s_2, \gamma, Q} \quad & \gamma && \text{(50a)} \\ \text{subject to} \quad & \text{(44b)}, \text{(44c)}, \text{(44d)}, \text{(44e)}, && \text{(50b)} \\ & \operatorname{tr}(Q(\tau)) = c(\tau), \quad \forall \tau \in \mathcal{I}_T^\circ. && \text{(50c)} \end{aligned}$$

4.2.3. *Scaling the ellipsoid inside a variable-degree-V sublevel set (referred to as SE-$\partial(r)$).* It is well-known that higher degree Lyapunov functions have the potential to verify larger ROA estimates [40, 44, 3]. In this algorithmic option, the Lyapunov function is thus parametrized as

$$V(\tau, \rho) = \mathrm{v}(\rho)^T Q(\tau) \mathrm{v}(\rho), \tag{51}$$

where $\mathrm{v}(\rho)$ is the monomial vector in ρ up to degree $r/2$, with $r \geq 2$. In order to formally define the objective of maximizing the volume of $\mathcal{R}$, a fixed shape surrogate set is considered. Its size is then maximized, subject to the constraint that the surrogate set lies inside of $\mathcal{R}$. This approach is similar to the method proposed in [23] in the context of ROAs of equilibrium points. Here we propose a generalization of this approach to Lyapunov functions for periodic orbits. The surrogate set is given by the sublevel set of a quadratic function $b = \rho^T B_F \rho$

$$\mathcal{B}_F = \{\rho \in \mathbb{R}^{n-1} \,|\, b(\rho) \leq \alpha\}, \tag{52}$$

where $B_F \in \mathbb{R}^{(n-1)\times(n-1)}$ is a fixed positive definite matrix prescribing the shape of the elliptical surrogate set. The constraint that $\mathcal{B}_F \subseteq \mathcal{R}$ is a set containment condition and can thus be enforced as is done for the others. The associated optimization problem is

$$\begin{aligned} \max_{s_1, s_2, s_3, Q} \quad & \alpha && \text{(53a)} \\ \text{subject to} \quad & -(\alpha - b(\rho))\, s_3(\tau, \rho) + (1 - V(\tau, \rho)) \in \Sigma[\tau, \rho], && \text{(53b)} \\ & \text{(44b)}, \text{(44c)}, \text{(44d)}, \text{(44e)}, && \text{(53c)} \end{aligned}$$

where $s_3(\tau, \rho)$ is an additional SOS multiplier. Note that in this option the scaling factor of a single fixed shape ellipsoid is maximized while the ellipsoid is constrained to lie inside the τ-varying 1-sublevel set of V. This simultaneously maximizes the sublevel set of V since Q enters the optimization as decision variable. The size of the verified set $\mathcal{R}$ can depend significantly on the choice of the ellipsoid shape.

4.2.4. *Expanding the ellipsoid(s) inside a variable-degree-V sublevel set (referred to as EE-$\partial(r)$).* In order to circumvent the dependency of the verified set $\mathcal{R}$ on the choice of ellipsoid's shape, an extension of the SE-$\partial(r)$ approach is presented here. Specifically, a set with a shape which is not fixed a priori, but will be optimized over, is expanded inside $\mathcal{R}$. This surrogate set is taken as the sublevel set of a quadratic function $b(\tau, \rho) = \rho^T B(\tau) \rho$,

$$\mathcal{B} = \{(\tau, \rho) \in \mathcal{I}_T^\circ \times \mathbb{R}^{n-1} \,|\, b(\tau, \rho) \leq 1\}, \tag{54}$$

with a fixed sublevel set scaling factor. The matrix $B(\tau) \in \mathbb{R}^{(n-1)\times(n-1)}$ is constrained to be positive definite and its entries enter as decision variables into (44). The objective is to maximize the size of the set (54), and thus one would want to minimize $\det\big(B(\tau)\big)$, which represents the inverse of its volume. However, this is a non-convex function, and thus we resort here to a common heuristic in minimum

volume ellipsoid problems. Precisely, to preserve tractability of the optimization problem, we consider the trace of B [8], which is inversely proportional to the sum of the principal axes of the ellipsoidal set. Since the goal here is to maximize the size of the ellipsoid defined by B, it is proposed to minimize $\mathrm{tr}\,(B)$. The associated optimization problem is

$$\min_{s_1,s_2,s_3,Q,B} \quad \mathrm{tr}\,(B) \tag{55a}$$

$$\text{subject to} \quad -(1-b(\tau,\rho))\,s_3(\tau,\rho)+(1-V(\tau,\rho)) \in \Sigma[\tau,\rho], \tag{55b}$$

$$(44b), (44c), (44d), (44e), \tag{55c}$$

It is noted that whereas $\mathrm{tr}\,(B)$ is only a surrogate of the volume of the ellipsoid, numerical tests suggest that it performs better than other metrics, such as the geometric mean of the eigenvalues of B, which would lead to less tractable formulations.

An interesting variation of this option, considered later in the analysis and aimed at reducing the computational complexity, consists of considering a constant B which is independent of τ. In this way, the importance of a variably expanding ellipsoid compared to a fixed shape surrogate set can be assessed. In terms of notation, the variant for the option with the τ-varying B is indicated by the subscript m (EE-$\partial(r)_m$), and the τ-independent B variant by s (EE-$\partial(r)_s$).

It is emphasized that the algorithmic options considered here are not exhaustive. However, in terms of complexity and range of resulting estimate sizes, they cover an interesting range of possible objective function choices having a noticeable impact, as investigated in Section 5.

We conclude this section by providing some more detail on the implementation of the optimization programs. In all the algorithmic options presented above, the resulting SOS programs have constraints featuring bilinear terms in the decision variables. A coordinate descent approach is used here, whereby one successively minimizes the objective function by optimizing over different variables. Namely, we alternate between V and s_1, s_2, s_3. The original optimization problem is therefore solved iteratively by a sequence of SDPs.

An important feature, specific to the limit cycle ROA problem, is that, due to the dependency on the time-like variable τ, the program has a time-varying nature. Since this leads to a significant computational complexity, accuracy of the solution can be traded for computational efficiency by solving the problem for a discrete set of τ (of length N) within the full interval $[0,T]$ [43]. This effectively chooses a set of fixed transversal hyperplanes on which the conditions of Theorem (4.1) are tested. Note that, the finer is the sampling of τ, the greater is the accuracy of the solution, but the higher is the computational cost due to the added constraints for each hyperplane. The τ-sampled polynomials are denoted with a superscript i in the following.

The piecewise linear Lyapunov function obtained by sampling τ is indicated as

$$V^{(i)}(\rho) := \mathrm{v}(\rho)^T Q^{(i)} \mathrm{v}(\rho), \tag{56}$$

The explicit expression of its τ-derivative is

$$\frac{\partial V^{(i)}(\rho)}{\partial \tau} = \mathrm{v}(\rho)^T \left(\frac{Q^{(i+1)} - Q^{(i)}}{\tau^{(i+1)} - \tau^{(i)}} \right) \mathrm{v}(\rho), \quad i = 1, ..., N\text{-}1. \tag{57}$$

The constraint (44b) is automatically satisfied by enforcing $Q^{(i)} \succ 0$. The τ-sampled optimization program for the algorithmic option EE-$\partial(r)_m$ results in the following

SOS program.

$$\min_{s_1^{(i)},s_2^{(i)},s_3^{(i)},Q^{(i)},B^{(i)},i=1\ldots N-1} \quad \sum_{i=1}^{N-1} \operatorname{tr}\left(B^{(i)}\right)^{1/(n-1)} \tag{58a}$$

$$\text{subject to} \quad -\dot{V}^{(i)}(\rho) - \left(1 - V^{(i)}(\rho)\right) s_1^{(i)}(\rho) - l(\rho) \in \Sigma[\rho], \tag{58b}$$

$$\eta^{(i)}(\rho) - \left(1 - V^{(i)}(\rho)\right) s_2^{(i)}(\rho) \in \Sigma[\rho], \tag{58c}$$

$$-\left(1 - b^{(i)}(\rho)\right) s_3^{(i)}(\rho) + \left(1 - V^{(i)}(\rho)\right) \in \Sigma[\rho], \tag{58d}$$

$$s_1^{(i)}(\rho), s_2^{(i)}(\rho), s_3^{(i)}(\rho) \in \Sigma[\rho], \tag{58e}$$

$$Q^{(i)} \succ 0. \tag{58f}$$

The implementation of the iterative steps to solve (58) is shown in Algorithm 1. The iteration is initialized by solving the periodic Lyapunov equation (46) for the transverse linearization of the dynamics and scaling the result via bisection until SOS multipliers certifying (58b)-(58e) are found. Since the initial Lyapunov function is quadratic, a feasible surrogate set can always be found by proper scaling. In Step 1, the Lyapunov function is kept fixed and, for each $\tau^{(i)}$, a feasibility test consisting of (58b)-(58e) is performed to obtain the SOS multiplier for that $\tau^{(i)}$. The problem for each $\tau^{(i)}$ sample is independent from the others, and so $N-1$ feasibility tests (the first and last points of the grid coincide) are performed in parallel in this step. In Step 2, the problem on each hyperplane depends on the neighboring ones due to the Lyapunov derivative. Thus, for each $\tau^{(i)}$, the multipliers are fixed and the constraints on V are added to a single large optimization program. In this second step the degree of the Lyapunov function can be increased to the desired order. Steps 1 and 2 are repeated until the maximum increase of the expanding ellipsoids on the hyperplanes falls below a specified threshold (convCrit_B in Algorithm 1).

Note finally that by appropriately replacing the cost function and constraints, Algorithm 1 can be used for any of the algorithmic options presented above.

5. Numerical examples.

This section illustrates the application of the ROA analysis to three case studies comprising two planar systems and an airborne wind energy system in the power generating phase. In addition to showing the succesful application of the proposed method, this section offers two important types of comparison: one concerning the impact of the adopted MOC (either class-MOC or cp-MOC) and the other relative to the algorithmic options for the ROA computation. The scripts used to perform the analyses are available in the repository [1], and all the SOS problems are solved using Yalmip's built-in module for sum-of-squares calculations [28, 27].

5.1. Van der Pol oscillator.

The Van der Pol oscillator dynamics [26] are defined by the following system of ordinary differential equations

$$\begin{aligned} \dot{x}_1 &= x_2, \\ \dot{x}_2 &= (1 - x_1^2)x_2 - x_1. \end{aligned} \tag{59}$$

This system has a unique stable limit cycle Γ_{VDP} which encircles an unstable equilibrium point at $x_{\text{EP}} = [0,0]^T$. The ROA of Γ_{VDP} thus includes all of $\mathbb{R}^2 \backslash \{x_{\text{EP}}\}$.

We use this example to investigate the effect of the choice of the MOC and the effect of different degrees of Lyapunov functions on the ROA estimates $\mathcal{R}$. For this

Algorithm 1 Find Lyapunov function for orbit to maximize $\mathcal{R}$

Input: N, $\partial(s_1^{(i)})$, $\partial(s_2^{(i)})$, $\partial(s_3^{(i)})$, $\partial(V^{(i)})$, convCrit_B
Output: V, $\mathcal{R}$
procedure MAXROAESTIMATE
    $\dot{\rho}$, $\dot{\tau}$ $\xleftarrow{(37),(35)}$ $f(x)$, $\omega(t)$
    Initialization:
    $Q_{\text{ini}}(\tau) \leftarrow c \cdot P(\tau)$ solution of (46), bisect c such that (58b)-(58e) feasible
    ${Q_{\text{ini}}}^{(i)} \leftarrow Q_{\text{ini}}(\tau_i)$
    choose $B^{(i)}$ small enough such that (58d) is feasible
    Iteration:
    $k \leftarrow 0$
    repeat
        $k \leftarrow k + 1$
        for $i = 1 : N\text{-}1$ **do**
            Step 1: $s_1^{(i)}$, $s_2^{(i)}$, $s_3^{(i)} \leftarrow$ fix $Q^{(i)}$, $B^{(i)}$ solve (58b)-(58e)
        end for
        Step 2: $Q^{(i)}$, $B^{(i)}$, $_{i=1\ldots N\text{-}1} \leftarrow$ fix $s_1^{(i)}$, $s_2^{(i)}$, $s_3^{(i)}$, $_{i=1\ldots N\text{-}1}$ solve (58a)-(58d)
    until $\max\{\det(B^{(i)})_{k-1} - \det(B^{(i)})_k\}_{i=1}^{N-1} < \text{convCrit}_B$
end procedure

purpose we use the option EE-$\partial(r)_m$ in the Algorithm 1 and fix the multiplier to $\partial(s_1) = 6$, $\partial(s_2) = 2$ and $\partial(s_3) = 2$. Figure 3 shows the volume of the computed $\mathcal{R}$ as a function of τ for the four cases of a quadratic and a quartic Lyapunov function used in conjunction with class-MOC and cp-MOC. The computations are performed using $N = 50$, giving 49 distinct hyperplanes (recall that $\tau_1 = \tau_{50}$). As can be seen in the plot, the ROA estimates are significantly larger for the cp-MOC than for the class-MOC. Furthermore, as expected, for both MOCs the quartic Lyapunov function returns on average a larger $\mathcal{R}$ than the quadratic. The center point for these analyses is $x_c = [0, 0]^T$.

Figure 4 provides insights into the marked difference in the size of the estimates $\mathcal{R}$ corresponding to the two MOC (left plot is for class-MOC and right plot is for cp-MOC). The center point is $x_c = [0, 0]^T$. The results for quartic Lyapunov function are overlaid with those for quadratic Lyapunov function. This figure reveals the reason for the significantly smaller ROA estimates obtained with class-MOC, which is a consequence of Corollary 2. That is, the intersection of neighboring hyperplanes, which represents the limit point of the well-definedness of the transverse coordinate transformation (11), precludes finding larger sets $\mathcal{R}$. In the case of cp-MOC the hyperplanes all intersect in the single point x_c which allows much larger regions $\mathcal{R}$ to be found by Algorithm 1 in this example.

5.2. **Dual-orbit system.** The goal of this case study is to investigate in detail the effect of the different algorithmic options proposed in Section 4.2 on the quality of the inner approximations of the true ROA. The system has a locally stable limit cycle and is obtained by modifying a version of the Liénard system presented in [15]

$$\begin{aligned} \dot{x}_1 &= -x_2 + 3x_1(x_1^2 - 1/4)(x_1^2 - 1), \\ \dot{x}_2 &= x_1. \end{aligned} \tag{60}$$

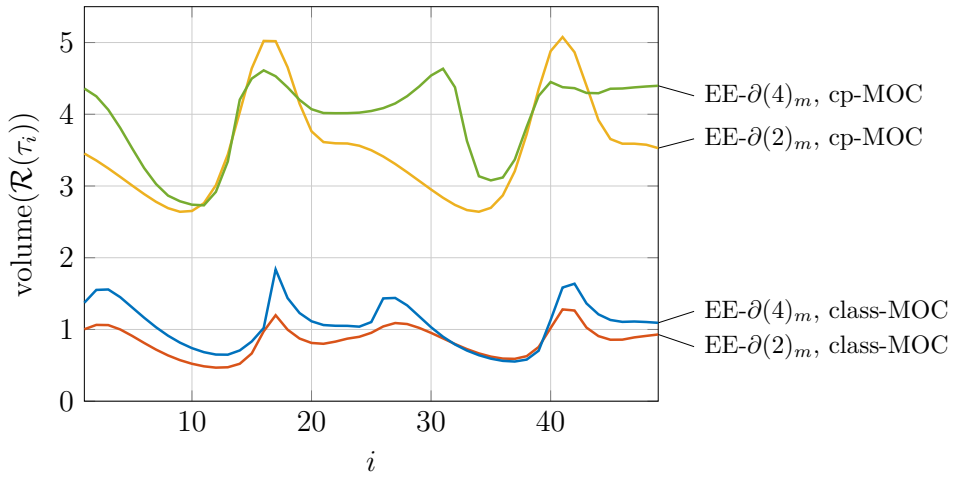

FIGURE 3. Comparison of $\mathcal{R}$ sizes obtained from Algorithm 1 for the algorithmic choice EE-$\partial(r)_m$ where both quadratic and quartic Lyapunov functions were used for class-MOC and cp-MOC.

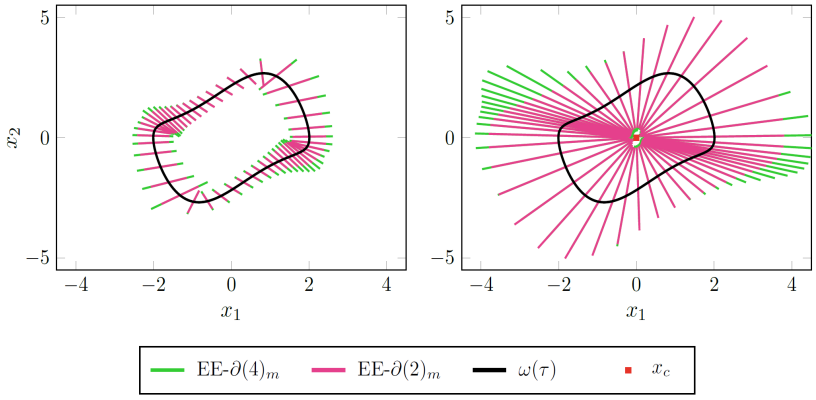

FIGURE 4. Illustration of the computed ROA estimates shown in Figure 3 for the Van der Pol oscillator (59). The results for the quartic Lyapunov function are overlaid with those for the quadratic. *Left plot:* ROA estimates for the class-MOC. *Right plot:* ROA estimates for the cp-MOC.

The main modification consists of reducing the degree of the polynomials from 7 to 5. This was done to lower the complexity of the SOS optimization problems, and its only effect was to eliminate the outermost stable LC, with no effect on the dynamical behaviour of interest for these analyses. In the form considered here the system has two LCs of which one is encircling the other. The inner one, denoted by Γ^A_{dual}, is an attractive LC around the unstable equilibrium point $x_{\text{EP}} = [0, 0]^T$. The outer one is an unstable LC and is denoted by Γ^U_{dual}. Figure 5 shows a phase portrait of the system in the neighborhood of the LCs. The true ROA of Γ^A_{dual} is given by the region encircled by Γ^U_{dual} (excluded x_{EP}).

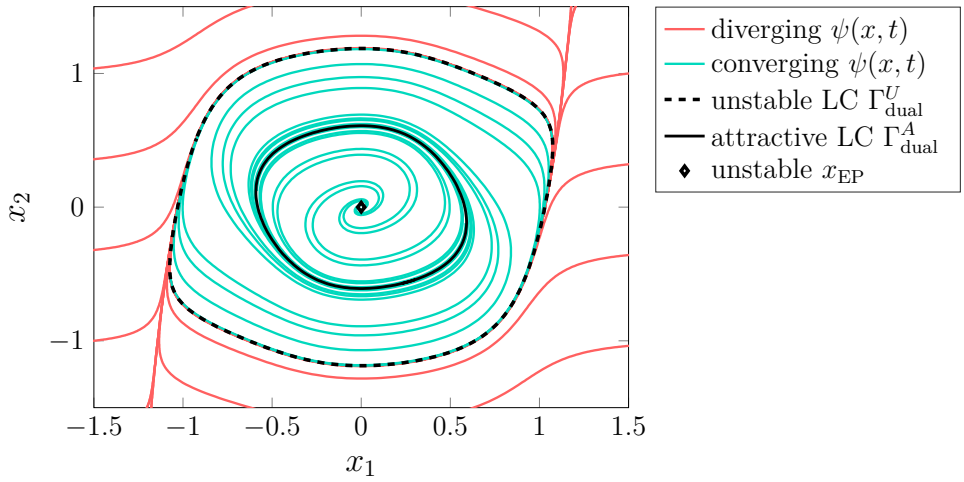

FIGURE 5. Phase portrait of the dual-orbit system (60) in the neighborhood of the attractive and unstable LCs. The green lines show examples of converging trajectories while the red lines represent diverging ones.

For this system, all algorithmic options presented in Section 4.2 were used to compute a ROA estimate for both the class-MOC and cp-MOC. For the two options SE-$\partial(r)$ and EE-$\partial(r)$, which allow for higher order Lyapunov functions, the cases of a quadratic and a quartic function were both considered. The multiplier degrees were fixed for all options to $\partial(s_1) = 6$, $\partial(s_2) = 2$, and $\partial(s_3) = 2$. Each estimate was obtained for the same range of 50 discrete values of $\tau \in [0, T]$. The aim of the comparison is to investigate the differences in the outcome among the algorithmic choices as well as to analyze the conservativeness of the results with respect to the true ROA. The center point coincides with x_{EP}.

The volumes for the computed $\mathcal{R}$ are shown as a function of τ in Figures 6 for the class-MOC and in Figure 7 for the cp-MOC. Both figures reveal that larger sets $\mathcal{R}$ are obtained with higher degree Lyapunov functions and with more flexible cost functions definitions. Indeed, $\mathcal{R}$ obtained from VSS-∂_{lin} is significantly smaller than all other estimates as its only flexibility consists of the uniform scaling of the Lyapunov sublevel set obtained for the linearized system. Allowing the shape of this sublevel set to vary results in significantly larger estimates, as the sets $\mathcal{R}$ obtained for VSS-$\partial(2)$ show. This option still only considers quadratic Lyapunov functions and the cost function is equal to the one in VSS-∂_{lin} while the computational complexity is significantly increased due to the constraints on Q and added decision variables.

In both cases, the results from the algorithmic options involving quadratic Lyapunov functions (except for VSS-∂_{lin}) give very similar results. While for the class-MOC the use of a surrogate set in the options SE-$\partial(2)$, EE-$\partial(2)_s$ and EE-$\partial(2)_m$ results in small increases compared to VSS-$\partial(2)$, these are negligibly small in the results for cp-MOC. The more significant benefit of using surrogate sets is clearly shown in the comparison of the results obtained for the quadratic Lyapunov function compared to the results of the quartic one, where the latter almost always shows better results. Another important aspect, confirming the results of the Van

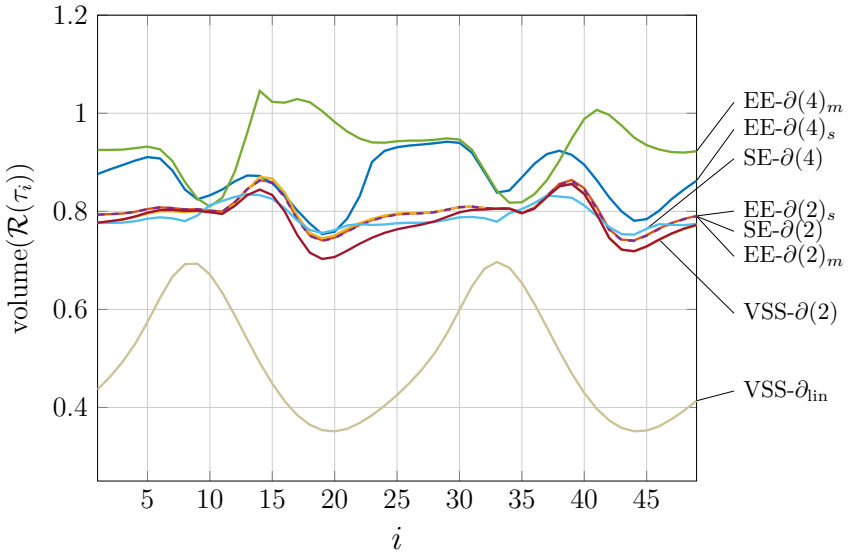

FIGURE 6. ROA estimates as a function of τ, obtained from the different algorithmic choices presented in 4.2 for the class-MOC.

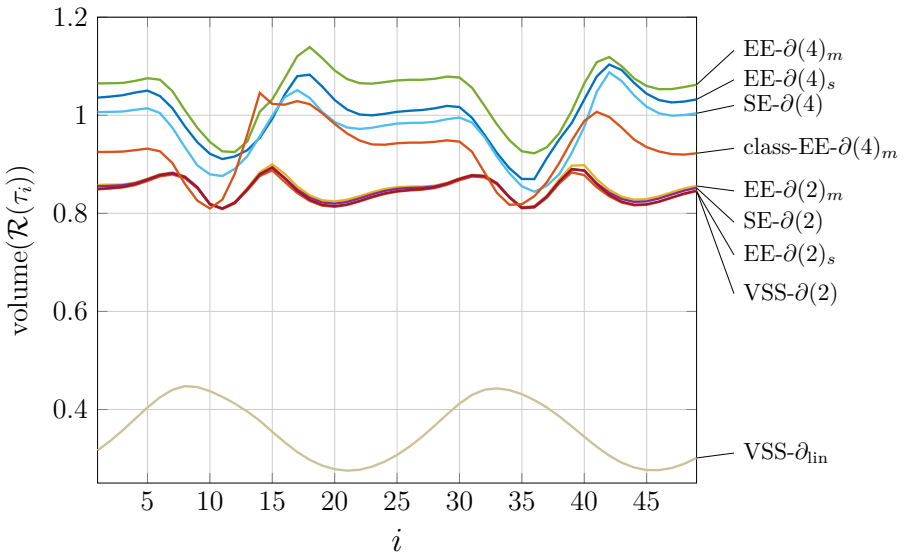

FIGURE 7. ROA estimates as a function of τ, obtained from the different algorithmic choices presented in 4.2 for the cp-MOC. For comparison, the EE-$\partial(4)_m$ result obtained for the class-MOC is included.

der Pol oscillator, is that cp-MOC provides, for all the algorithmic options (except for VSS-∂_{lin}), larger regions.

Figure 8 illustrates the sets $\mathcal{R}$ for EE-$\partial(4)_m$ and VSS-$\partial(2)$ on the 49 chosen hyperplanes for the class-MOC (left plot) and the cp-MOC (right plot). The results

TABLE 1. Comparison of iteration numbers obtained for the dual orbit example for each algorithmic option and MOC.

Algorithmic option	class-MOC		cp-MOC	
	$\partial(V)=2$	$\partial(V)=4$	$\partial(V)=2$	$\partial(V)=4$
EE-$\partial(r)_m$	23	51	20	49
EE-$\partial(r)_s$	10	9	8	8
SE-$\partial(r)$	39	32	39	33
VSS-$\partial(2)$	12	-	12	-
VSS-∂_{lin}	10	-	6	-

for EE-$\partial(4)_m$ are overlaid with those for VSS-$\partial(2)$. The figure shows that both MOC enable the EE-$\partial(4)_m$ to obtain ROA estimates which are very close to the size of the true ROA towards its outer boundary. While due to the intersection of hyperplanes in the class-MOC case the estimates are not covering the neighborhood of x_{EP}, this limitation does not hold for cp-MOC, where the ROA can also be certified in regions close to x_{EP}.

Table 1 lists the number of iterations performed for each algorithmic option, choice of MOC and Lyapunov function degree. The comparison shows that there were significant differences between the algorithmic options, variations among different Lyapunov function degrees and comparably little variation between the two choices of MOC. By combining the volume plot results with the iteration numbers it can be seen that the larger sized ROA estimate obtained for the option EE-$\partial(r)_m$ comes at the cost of a significantly higher number of iterations than its less flexible counterpart EE-$\partial(r)_s$ needed for a slightly smaller sized ROA estimate. It is noted that the runtime of the proposed algorithms is dominated by the number of states and highest polynomial degree and far less by the differences among the algorithmic options. The number of iterations needed until convergence, however, varies strongly among the options.

Remark 6. Figure 8 provides an interesting insight onto the advantage of the cp-MOC with respect to the class-MOC. Even though for class-MOC the estimates are only close to the hyperplane intersection point for a few values of τ, the algorithm can not efficiently increase the estimates on the hyperplanes on which the estimates are still far from the intersection point. This happens even when there is a higher flexibility for shaping the surrogate sets on each hyperplane, as it is the case with the option EE-$\partial(4)_m$. The reason for this is due to the fact that the coordinate frame used for the transverse coordinates determines an inherent limitation on the verifiable ROA of the limit cycle. Indeed, if some initial conditions cannot be verified in some hyperplanes (because the well-defined region is too small), other initial conditions lying on other hyperplanes (possibly with a larger well-defined region) and crossed by trajectories originating from the other initial conditions, will not be verifiable either. This creates a particular coupling between the hyperplanes and the verification of inner estimates of the ROA which depends on the dynamcs. The cp-MOC is better able to cope with this because it allows the analyst to design the hyperplanes in such a way that the well-defined sets $\mathcal{V}_\tau$ are more similar in size.

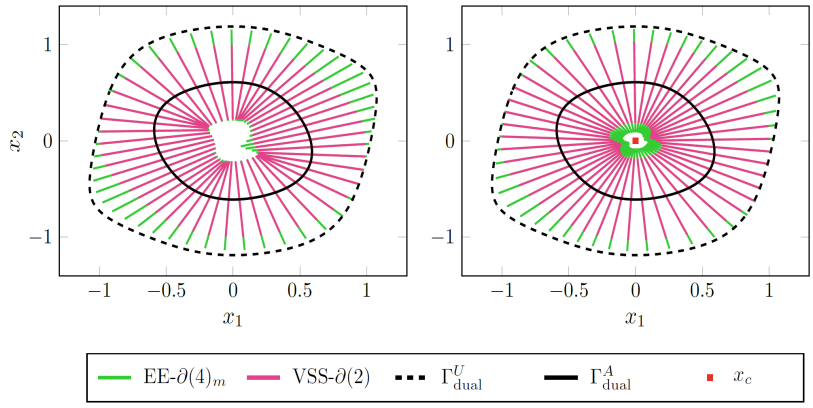

FIGURE 8. Illustration of selected ROA estimates shown in Figure 6 and Figure 7 for the dual-orbit system (60). The results for the quartic Lyapunov function are overlaid with those for the quadratic. *Left plot:* ROA estimates for the class-MOC. *Right plot:* ROA estimates for the cp-MOC.

5.3. **Stabilized Airborne Wind Energy system.** The analysis considered in this example investigates the regions of the state space in which a transverse feedback controller is able to stabilize an Airborne Wind Energy system in the power-generating phase. The model of the kite system, the desired reference trajectory and the transverse controller are taken here from [4]. The states are $x = (\theta, \phi, \gamma)$, where θ denotes the elevation angle, ϕ the azimuth angle, and γ the orientation angle of the kite. The system dynamics can be described by

$$\begin{aligned} \dot{\theta} &= \frac{v_k}{L}\cos(\gamma), \\ \dot{\phi} &= \frac{v_k}{L}\cos(\theta)^{-1}\sin(\gamma), \\ \dot{\gamma} &= v_k G u, \end{aligned} \tag{61}$$

where L is the tether line length, $v_k = v_w E\cos(\theta)\cos(\phi)$ is the wind velocity, and $E = C_L/C_D$ is the glide ratio with C_L denoting the lift coefficient and C_D the drag coefficient. Further, G is the steering gain and u is the control input.

The reference trajectory of the system is denoted by $\tilde{x}(\tau)$. The system parameters are set to $L = 60$ m, $E = 5.7$, $v_w = 6$ m/s, and $G = 1.25$. The parameter G was obtained from a rough approximation of the steering gain derived from first principles as proposed in [13]. For the τ-discretization, 50 evenly spaced discrete values of τ were chosen over the period $[0, T]$, where $T = 5$ s.

Since the SOS verification methods require the system to be in polynomial form, the closed-loop system is approximated by a third-order Taylor series around $\tilde{x}(\tau)$.

The kite system provides an example for the cp-MOC for a three dimensional system. Figure 9 illustrates 8 randomly selected hyperplanes $\mathcal{S}(\tau_i)$ in the cp-MOC for the reference trajectory. The plots show how all hyperplanes intersect in a 1-dimensional subspace consisting in a line through the center point which was chosen at $x_c = [0.3, 0, 0]^T$. The rotation in the left plot was chosen such that the intersection line points out of the plane.

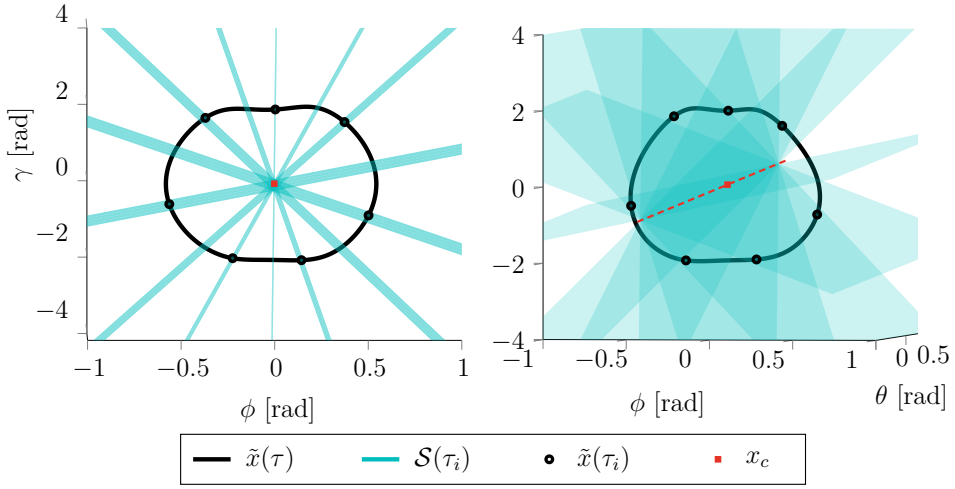

FIGURE 9. Illustration of the hyperplanes in the cp-MOC from two different angles. In the right plot, the red dashed line indicates the 1-dimensional subspace given by the intersection of the hyperplanes. In the left plot, this collpases to a point.

Figure 10 presents the results of the ROA analyses. The volume of the set $\mathcal{R}$ was numerically obtained by fitting a polygon with 80 edges into the verified sublevel set of $V(\tau, \rho)$, which for 3-dimensional system is a planar region on each hyperplane. In order to obtain a meaningful comparison across these different algorithmic options, certain parameters, such as the degrees of the SOS-multipliers, were fixed for all options.

Similar characterizations to those already discussed for the previous two examples can be observed. A peculiar feature, seen in class-MOC for both degrees of V, is a spike for $i = 14$. For these hyperplanes, the curvature of the kite trajectory is very small, which leads to the well-defined regions of the transformation being very large. Due to the flexibility of EE-$\partial(r)_m$ in adjusting the objective function individually for each hyperplane, the algorithm takes advantage of these particularly large sets in this case. The small sizes of the results for SE-$\partial(r)$ for all MOCs and V functions show the potentially detrimental effect of a surrogate set which is fixed in shape and could not be pre-adjusted to the shape of the sublevel set of $V(\tau_i, \rho)$ due to lack of information.

The iteration numbers for each case are listed in Table 2. In particular the comparison with the iteration number for the 2-dimensional dual orbit example in Section 5.2 shows that the option EE-$\partial(r)_s$ was again among the options requiring a comparably low number of iterations. While the option EE-$\partial(r)_m$ for the class-MOC and quartic Lyapunov function gave the largest ROA estimates the number of iterations required is also significantly higher than for most other options. For the class-MOC, the number of iterations for the option SE-$\partial(r)$ is again very high, as in the dual orbit example. They are acceptable for the cp-MOC, but the estimates obtained are comparably small. This highlights the disadvantage of this algorithmic option, owing to the fact that the shape of the surrogate set is fixed.

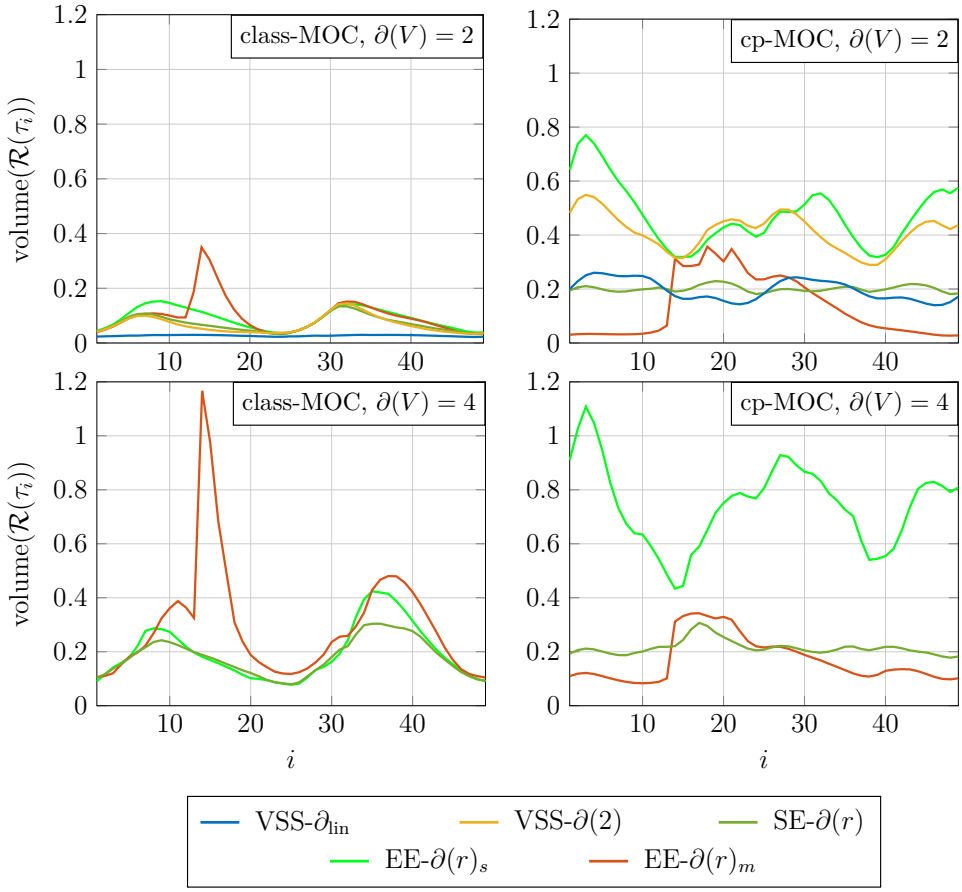

FIGURE 10. Results showing the volume of $\mathcal{R}$ on each of the 49 selected distinct hyperplanes $\mathcal{S}(\tau_i), i = 1, ..., 49$, obtained from the different algorithmic options in Section 4.2 and from both presented options of MOC in Section 2.3. A quadratic and a quartic (where applicable) Lyapunov function were used.

Figures 11 and 12 illustrate the region $\mathcal{R}$ obtained from EE-$\partial(4)_s$ on each of the selected 49 hyperplanes in a 3-dimensional plot for both the choice of the class-MOC and the cp-MOC. The plots highlight the significantly larger regions obtained with the cp-MOC choice of moving coordinate system. Figure 12 reveals that the algorithm was able to verify the stability of the system on regions extending close to the boundaries of the well-defined regions $\mathcal{V}_\tau$. The plots show also that the intersecting sets for the class-MOC are much closer to the trajectory $\tilde{x}(\tau)$ around the extreme values of ϕ, while for the cp-MOC all hyperplanes intersect in a single line which goes through the center point, as shown in Fig. 9.

6. **Conclusion.** In this work the novel construction of a moving orthonormal coordinate system based on a user defined center point is proposed. Its main appealing feature is that it improves the well-definedness properties for transverse coordinates compared to classical approaches. Based on this center point coordinate system and

TABLE 2. Comparison of iteration numbers obtained for the deterministic kite example for each algorithmic option and MOC.

Algorithmic option	class-MOC		cp-MOC	
	$\partial(V)=2$	$\partial(V)=4$	$\partial(V)=2$	$\partial(V)=4$
EE-$\partial(r)_m$	19	44	11	10
EE-$\partial(r)_s$	10	18	15	19
SE-$\partial(r)$	54	27	18	15
VSS-$\partial(2)$	8	-	12	-
VSS-∂_{lin}	7	-	14	-

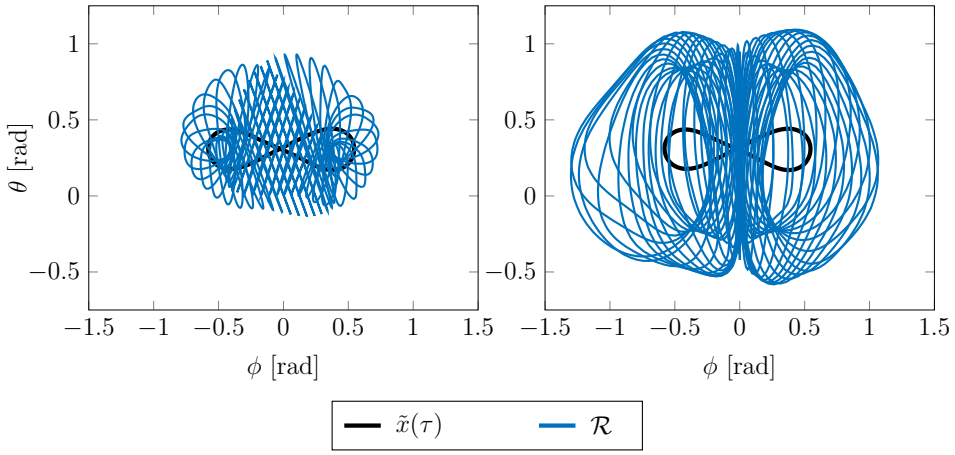

FIGURE 11. Results showing $\mathcal{R}$ obtained from EE-$\partial(4)_s$, plotted on each corresponding hyperplane. The ϕ-θ plane of the 3-dimensional plot is shown. *Left plot:* Results for the class-MOC. *Right plot:* Results for the cp-MOC.

Lyapunov stability arguments, conditions for numerically computing inner estimates of the region of attraction of a limit cycle are formulated in terms of sum-of-squares optimization. Various algorithmic options are presented to reduce conservatism of the inner estimates and extensive results obtained on three numerical examples demonstrate their features. The presented work opens us interesting future directions. Algorithm 1 can be directly extended to systems with affine input for a control design which aims at maximizing the ROA of the limit cycle. As shown in the kite example, the transverse coordinate transformation does not alter the affine dependence on the control gain. Furthermore, as shown in Theorem 3.3, the center point can be freely chosen inside an appropriate set, which was analytically defined in this paper. One can thus consider an optimization problem for the center point location and the $(n\text{-}2)$ dimensional subspace $\mathcal{N}_f$ with the aim of maximizing the verifiable ROA estimate. Whereas the proposed algorithmic options relax to some extent the computational burden of the programs, scalability issues with SOS program remain a limiting factor of the proposed approach for estimating inner estimates of the ROA. In this regard, recently proposed relaxations [5] and sparsity-exploiting algorithms [51] can ameliorate these known problems. We observe that

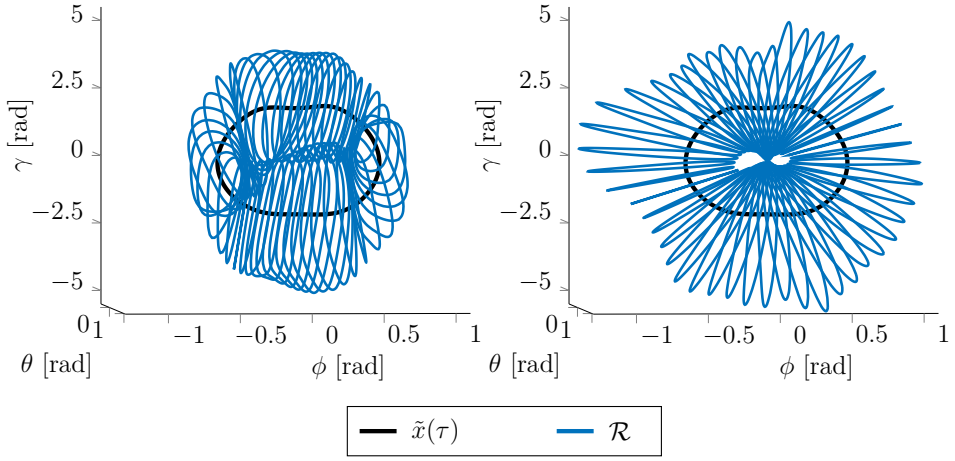

FIGURE 12. Rotated view of the plots in Figure 11. *Left plot:* Results for the class-MOC. *Right plot:* Results for the cp-MOC.

state-of-the-art SOS solvers such as SOSTOOLS [33] have included some of these utilities in their latest releases.

ACKNOWLEDGEMENTS. The authors would like to thank the anonymous reviewers for their remarks and suggestions, which greatly contributed to improving the paper.

APPENDIX. The proof of Theorem 2.4 [17] is given here because it shows the construction of the class-MOC system.

Suppose $n \geq 3$. If $v(\tau) = f(\omega(\tau))\|f(\omega(\tau))\|_2^{-1}$, then the hypotheses on ω imply that v is periodic of period T and Lipschitz. Let $e_1 = \zeta^*$ be a constant unit vector (the existence of which is assured by Lemma 2.3) such that $e_1 \neq \pm v(\tau)$, $0 \leq \tau \leq T$. Adjoin to e_1 any constant vectors $e_2, ...e_n$ such that $\{e_1, e_2, ...e_n\}$ is an orthonormal basis for $\mathbb{R}^n$. The moving orthonormal system along Γ is then obtained in the following manner: Let S be the $(n-2)$-dimensional subspace of $\mathbb{R}^n$ orthogonal to the plane formed by e_1 and $v(\tau)$. Rotate the coordinate system about S in the positive sense until e_1 coincides with $v(\tau)$. If $\zeta_1, \zeta_2, ..., \zeta_n$ are the rotated positions of $e_1, e_2, ...e_n$, then the moving orthonormal system is given by

$$\{v(\tau), \zeta_2(\tau), ..., \zeta_n(\tau)\}, \quad 0 \leq \tau \leq T, \tag{62}$$

where $\zeta_1(\tau) = v(\tau)$.

If $\gamma_j(\tau)$, $j = 1, 2, ..., n$ are the direction angles of $v(\tau)$, $e_j \cdot v(\tau) = \cos(\gamma_j(\tau)$, $j = 1, 2, ..., n$, then one can show that the vectors ζ_j are given by

$$\zeta_j(\tau) = \xi_j - \frac{\xi_j' v(\tau)}{1 + \xi_1 v(\tau)}(\xi_1 + v(\tau)), \quad j = 2, 3, ..., n. \tag{63}$$

The derivation of (63) is omitted for brevity and can be found in [17].

The proof then continues by treating the case $n = 2$. For this case, the moving orthonormal system is directly constructed as

$$\{v(\tau), \zeta_2(\tau)\}, \quad \zeta(\tau) = \pm[-v_2(\tau), v_1(\tau)]^T, \tag{64}$$

where $v_1(\tau), v_2(\tau)$ are the components of $v(\tau)$. The proof is concluded by observing that equations (62)-(64) for the class-MOC along Γ imply that the system is $\mathcal{C}^{p-1}(\mathbb{R}, \mathbb{R}^n)$, if ω is $\mathcal{C}^p(\mathbb{R}, \mathbb{R}^n)$.

REFERENCES

[1] Supplemental material to the paper "A novel moving orthonormal coordinate-based approach for region of attraction analysis of limit cycles", DOI: 10.3929/ethz-b-000492932, 2021, ETH Research Collection.

[2] E. Ahbe, T. A. Wood and R. S. Smith, Stability verification for periodic trajectories of autonomous kite power systems, in *IEEE European Control Conference*, 2018, 46–51.

[3] E. Ahbe, P. Listov, A. Iannelli and R. S. Smith, Feedback control design maximizing the region of attraction of stochastic systems using Polynomial Chaos Expansion, in *IFAC World Congress*, 2020.

[4] E. Ahbe, T. A. Wood and R. S. Smith, Transverse contraction-based stability analysis for periodic trajectories of controlled power kites with model uncertainty, in *IEEE Conference on Decision and Control*, 2018, 6501–6506.

[5] A. A. Ahmadi and A. Majumdar, DSOS and SDSOS Optimization: More Tractable Alternatives to Sum of Squares and Semidefinite Optimization, *SIAM Journal on Applied Algebra and Geometry*, **3** (2019), 193–230.

[6] U. Ahrens, M. Diehl and R. Schmehl, *Airborne Wind Energy*, Springer, Berlin, 2013.

[7] S. Bittanti, P. Colaneri and G. D. Nicolao, The Periodic Riccati Equation, in *The Riccati Equation* (eds. S. Bittanti, A. Laub and J. Williams), Springer, Berlin, 1991, 127–162.

[8] S. Boyd and L. Vandenberghe, *Convex Optimization*, Cambridge University Press, 2004.

[9] A. Chakraborty, P. Seiler and G. J. Balas, Nonlinear region of attraction analysis for flight control verification and validation, *Control Engineering Practice*, **19** (2011), 335–345.

[10] G. Chesi, Estimating the domain of attraction for non-polynomial systems via LMI optimizations, *Automatica*, **45** (2009), 1536–1541.

[11] G. Chesi, *Domain of Attraction Analysis and Control via SOS Programming*, London, U.K.: Springer, 2011.

[12] C. C. Chung and J. Hauser, Nonlinear control of a swinging pendulum, *Automatica*, **31** (1995), 851–862.

[13] L. Fagiano, A. U. Zgraggen, M. Morari and M. Khammash, Automatic crosswind flight of tethered wings for airborne wind energy: modeling, control design and experimental results, *IEEE Transactions on Control Systems Technology*, **22** (2014), 1433–1447.

[14] L. B. Freidovich and A. S. Shiriaev, Transverse Linearization for Underactuated Nonholonomic Mechanical Systems with Application to Orbital Stabilization, in *Distributed Decision Making and Control*, Springer-Verlag London Limited, 2012, chapter 11, 245–258.

[15] A. Gasull and H. Giacomini, A new criterion for controlling the number of limit cycles of some generalized liénard equations, *Journal of Differential Equations*, **185** (2002), 54–73.

[16] P. Giesl, On the determination of the basin of attraction of periodic orbits in three- and higher-dimensional systems, *Journal of Mathematical Analysis and Applications*, **354** (2009), 606–618.

[17] J. K. Hale, *Ordinary Differential Equations*, R.E. Krierger Pub. Co., New York, 1980.

[18] J. Hauser and C. C. Chung, Converse Lyapunov functions for exponentially stable periodic orbits, *System & Control Letters*, **23** (1994), 27–34.

[19] A. Iannelli, A. Marcos and M. Lowenberg, Nonlinear Robust Approaches to Study Stability and Postcritical Behavior of an Aeroelastic Plant, *IEEE Transactions on Control Systems Technology*, **27** (2019), 703–716.

[20] A. Iannelli, A. Marcos and M. Lowenberg, Robust estimations of the Region of Attraction using invariant sets, *Journal of the Franklin Institute*, **356** (2019), 4622–4647.

[21] A. Iannelli, P. Seiler and A. Marcos, Region of attraction analysis with Integral Quadratic Constraints, *Automatica*, **109** (2019), 108543.

[22] Z. Jarvis-Wloszek, R. Feeley, W. Tan, K. Sun and A. Packard, Controls applications of sum of squares programming, in *Positive Polynomials in Control*, Springer, Berlin, Heidelberg, 2005, 3–22.

[23] Z. W. Jarvis-Wloszek, *Lyapunov Based Analysis and Controller Synthesis for Polynomial Systems using Sum-of-Squares Optimization*, PhD thesis, University of California, Berkeley, 2003.

[24] M. Jones and M. M. Peet, Using SOS for optimal semialgebraic representation of sets: Finding minimal representations of limit cycles, chaotic attractors and unions, in *Proceedings of the American Control Conference*, American Automatic Control Council, 2019, 2084–2091.
[25] G. A. Leonov, Generalization of the Andronov-Vitt theorem, *Regular and Chaotic Dynamics*, **11** (2006), 281–289.
[26] N. Levinson and O. K. Smith, A general equation for relaxation oscillations, *Duke mathmatical Journal*, **9** (1942), 382–403.
[27] J. Loefberg, YALMIP : A Toolbox for Modeling and Optimization in MATLAB, in *Proceedings of the CACSD Conference*, 2004.
[28] J. Löfberg, Pre- and post-processing sum-of-squares programs in practice, *IEEE Transactions on Automatic Control*, **54** (2009), 1007–1011.
[29] A. Majumdar and R. Tedrake, Funnel Libraries for Real-Time Robust Feedback Motion Planning, *The International Journal of Robotics Research*, **36** (2017), 947–982.
[30] I. R. Manchester, Transverse Dynamics and Regions of Stability for Nonlinear Hybrid Limit Cycles, in *IFAC Proceedings Volumes*, vol. 44, IFAC, 2011, 6285–6290.
[31] I. R. Manchester, M. M. Tobenkin, M. Levashov and R. Tedrake, Regions of Attraction for Hybrid Limit Cycles of Walking Robots, in *IFAC Proceedings Volumes*, IFAC, 2011, 5801–5806.
[32] J. Moore, R. Cory and R. Tedrake, Robust Post-Stall Perching with a Simple Fixed-Wing Glider using LQR-Trees, *Bioinspiration & biomimetics*, **9** (2014), 1–15.
[33] A. Papachristodoulou, J. Anderson, G. Valmorbida, S. Prajna, P. Seiler, P. A. Parrilo, M. M. Peet and D. Jagt, *SOSTOOLS: Sum of squares optimization toolbox for MATLAB*, `http://arxiv.org/abs/1310.4716`, 2021, Available from `https://github.com/oxfordcontrol/SOSTOOLS`.
[34] A. Papachristodoulou and S. Prajna, A Tutorial on Sum of Squares Techniques for Systems Analysis, in *Proceedings of the American Control Conference*, 2005, 2686–2700.
[35] A. Papachristodoulou and S. Prajna, Analysis of non-polynomial systems using the sum of squares decomposition, in *Positive polynomials in control*, 2005, 23–43.
[36] P. A. Parrilo, *Structured semidefinite programs and semialgebraic geometry methods in robustness and optimization*, PhD thesis, California Institute of Technology, 2000.
[37] S. Prajna, A. Papachristodoulou and F. Wu, Nonlinear Control Synthesis by Sum of Squares Optimization : A Lyapunov-based Approach, in *5th Asian Control Conference*, IEEE, 2004, 157–165.
[38] P. B. Reddy and I. A. Hiskens, Limit-induced stable limit cycles in power systems, *IEEE Russia Power Tech*, 1–5.
[39] G. Stengle, A Nullstellensatz and a Positivstellensatz in Semialgebraic Geometry, *Math. Ann*, **207** (1974), 87–97.
[40] W. Tan and A. Packard, Stability Region Analysis Using Polynomial and Composite Polynomial Lyapunov Functions and Sum-of-Squares Programming, *IEEE Transactions on Automatic Control*, **53** (2008), 565–571.
[41] J. Z. Tang, A. M. Boudali and I. R. Manchester, Invariant funnels for underactuated dynamic walking robots: New phase variable and experimental validation, in *IEEE International Conference on Robotics and Automation*, 2017, 3497–3504.
[42] R. Tedrake, I. R. Manchester, M. Tobenkin and J. W. Roberts, LQR-trees : Feedback Motion Planning via Sums-of-Squares Verification, *The International Journal of Robotics Research*, **29** (2010), 1038–1052.
[43] M. M. Tobenkin, I. R. Manchester and R. Tedrake, Invariant Funnels around Trajectories using Sum-of-Squares Programming, in *IFAC Proceedings Volumes*, vol. 44, IFAC, 2011, 9218–9223.
[44] U. Topcu, A. Packard and P. Seiler, Local stability analysis using simulations and sum-of-squares programming, *Automatica*, **44** (2008), 2669–2675.
[45] U. Topcu, A. Packard, P. Seiler and G. Balas, Help on sos [ask the experts], *IEEE Control Systems Magazine*, **30** (2010), 18–23.
[46] M. Urabe, *Nonlinear autonomous oscillations: Analytical theory.*, Academic Press, 1967.
[47] G. Valmorbida and J. Anderson, Region of attraction estimation using invariant sets and rational Lyapunov functions, *Automatica*, **75** (2017), 37–45.
[48] S. Wiggins, *Introduction to Applied Nonlinear Dynamical Systems and Chaos*, vol. 53, Springer-Verlag New York, 2003.

[49] T. A. Wood, H. Hesse, A. U. Zgraggen and R. S. Smith, Model-based flight path planning and tracking for tethered wings, in *IEEE Conference on Decision and Control*, 2015, 6712–6717.
[50] M. Wu, Z. Yang and W. Lin, Domain-of-attraction estimation for uncertain non-polynomial systems, *Communications in Nonlinear Science and Numerical Simulation*, **19** (2014), 3044–3052.
[51] Y. Zheng, G. Fantuzzi and A. Papachristodoulou, Chordal and factor-width decompositions for scalable semidefinite and polynomial optimization, *Annual Reviews in Control*, **.** (2021), .